

Linking Gulf Stream Air-Sea Interactions to the **exceptional** ~~blocking episode~~ Exceptional Blocking Episode in February 2019: A Lagrangian Perspective

Marta Wenta¹, Christian M. Grams¹, Lukas Papritz², and Marc Federer²

¹Institute of Meteorology and Climate Research, Department Troposphere Research (IMK-TRO), Karlsruhe Institute of Technology (KIT), Karlsruhe, Germany

²Institute for Atmospheric and Climate Science, ETH Zürich, Zurich, Switzerland

Correspondence: Marta Wenta (marta.wenta@kit.edu)

Abstract.

The development of atmospheric blocks over the North Atlantic European region can lead to extreme weather events like heatwaves or cold air outbreaks. Despite their potential severe impact on surface weather, the correct prediction of blocking lifecycles remains a key challenge in current numerical weather prediction (NWP) models. Increasing evidence suggests that latent heat release in cyclones, the advection of cold air (cold air outbreaks, CAOs) from the Arctic over the North Atlantic, and associated air-sea interactions over the Gulf Stream are key processes responsible for the onset, maintenance, and persistence of such flow regimes. ~~In order to establish how air mass transformations over the ocean, and in particular~~ To better understand the mechanism connecting air-sea interactions over the Gulf Stream, ~~–affect–~~ with changes in the large-scale flow, we focus on an episode between 20 and 27 of February 2019, when a quasi-stationary upper-level ridge was established over western Europe accompanied by an intensified storm track in the Northwestern North Atlantic. During that time, a record-breaking winter warm spell occurred over Western Europe bringing temperatures above 20°C to the United Kingdom, the Netherlands, and Northern France. The event was preceded and accompanied by the development of several ~~–~~ rapidly intensifying cyclones originating that originated in the Gulf Stream region and ~~traversing–traversed~~ the North Atlantic. To explore the mechanistic linkage between the formation of this block and air-sea interactions over the Gulf Stream, we adopt a Lagrangian perspective, using ~~backward and forward~~ kinematic trajectories. This allows us to study the pathways and transformations of air masses ~~forming that form~~ the upper-level potential vorticity anomaly and ~~interacting–interact~~ with the ocean front. We establish that more than one-fifth of these air masses interact with the Gulf Stream in the lower troposphere, experiencing intense heating and moistening over the region, due to the frequent occurrence of CAOs behind the cold front of the cyclones. Trajectories moistened ~~within the cold sector of~~ by the advection of cold air over warm ocean by one cyclone, later ~~ascent–ascend~~ into the upper troposphere with the ascending air stream of a consecutive cyclone, fueled by the strong surface fluxes. These findings highlight the importance of CAOs in the Gulf Stream region with their intense coupling between the ocean and atmosphere for blocking development ~~–~~ and provide a mechanistic pathway linking air-sea interactions in the lower troposphere and the upper-level flow.

1 Introduction

25 Atmospheric blocks are quasi-stationary anticyclonic circulation anomalies disrupting the eastward propagation of synoptic weather systems. The associated high-pressure system can dominate the weather over a particular location for an extended period of time, from several days to weeks (Wazneh et al., 2021) and lead to the development of extreme weather, like cold ~~surges~~ spells (e.g. de' Donato et al., 2013; Demirtaş, 2017; Pang et al., 2020; Zhuo et al., 2022) and heatwaves (e.g. Grumm, 2011; Barriopedro et al., 2011; Spensberger et al., 2020; Dae et al., 2022; Kautz et al., 2022) with significant socio-economic
30 impacts. Despite ongoing development and increasing resolution of numerical climate and weather prediction models, the correct prediction of those quasi-stationary weather patterns still poses a challenge (Matsueda and Palmer, 2018; Ferranti et al., 2018; Grams et al., 2018; Büeler et al., 2021).

The dynamics of cyclones and blocking anticyclones are mutually linked with the position and tilt of the upper-tropospheric jet. The crucial role of cyclones for the formation and maintenance of the blocks has been established by multiple studies (e.g. Colucci, 1985; Colucci and Alberta, 1996; Lupo and Smith, 1995; Nakamura and Wallace, 1993; Mullen, 1987; Yamazaki and Itoh, 2009). The development of cyclones results in the cross-isentropic ascent of air from the lower to the upper troposphere, in the so-called Warm Conveyor Belt (WCB; Wernli and Davies, 1997; Madonna et al., 2014; Pfahl et al., 2014). Condensation and resulting latent heat release during the ascent are critical for both cyclone intensification, through the production of potential vorticity (~~PV~~ PV) below the level of maximum heating (Binder et al., 2016; Reed et al., 1992; Čampa and Wernli, 2012), and
40 growth of the upper-level ridge, due to the destruction of PV above the level of maximum heating (Methven, 2015; Madonna et al., 2014; Joos and R.M.Forbes, 2016; Grams et al., 2011). The injection of low PV air into the upper troposphere together with diabatically enhanced divergent outflow amplifies and reinforces the upper-tropospheric ridge (Grams et al., 2011; Teubler and Riemer, 2016; Grams and Archambault, 2016; Steinfeld and Pfahl, 2019). Diabatic processes, as recently quantified by Pfahl et al. (2015); Steinfeld and Pfahl (2019); Steinfeld et al. (2020); Yamamoto et al. (2021) are in many cases essential for
45 the development of blocks in the North Atlantic-European region. In fact, recent studies indicate that the duration, strength, and possibly even formation of the block are influenced by latent heat release in the ascending ~~airstreams~~ air streams (Steinfeld et al., 2020; Pfahl et al., 2015).

The key role of moist dynamics in blocking formation and development suggests that there exists a relationship between up-stream, lower-tropospheric processes and the formation of the upper-level, quasi-stationary ridge. The air masses that undergo
50 latent heat release during the ascent in the warm sector of the cyclone need to first pass through ~~the~~ a region of intense surface evaporation to pick up a sufficient amount of moisture. Recent studies suggest that during winter the moisture source locations of cyclone precipitation are fairly local and over the ocean (Pfahl et al., 2014; Papritz et al., 2021). In the North Atlantic, the most intense evaporation events are associated with the Gulf Stream (Aemisegger and Papritz, 2018). The propagation of cyclones across the Gulf Stream region provides conditions for large surface latent and sensible heat fluxes (Tilinina et al.,
55 2018; Moore and Renfrew, 2002), due to the development of CAOs and the descent of dry air in the cold sector (Vanni re et al., 2017b; Raveh-Rubin, 2017; Aemisegger and Papritz, 2018). The warm waters of the Gulf Stream have been identified by Papritz et al. (2021) as a primary moisture source for cyclone-related precipitation in the North Atlantic. Papritz et al.

(2021) demonstrated also that air masses moistened and heated in the cold sector of one cyclone are then brought into the warm sector of the consecutive cyclone through a cyclone relative flow, called feeder ~~airstream (Dacre et al., 2019). Such air stream (Dacre et al., 2019). This type of~~ cyclone-cyclone interaction has ~~also been identified and labeled as been previously identified by Sodemann and Stohl (2013) and termed~~ a ‘hand-over’ mechanism ~~by Sodemann and Stohl (2013).~~ Furthermore, ~~Boutle et al. (2011) supports this understanding, having established that the moisture adjustment timescale in the boundary layer is approximately 2.3 days.~~ Moreover, intense turbulent heat fluxes during CAO events also play a crucial role in the restoration of baroclinicity in the lower troposphere (Papritz and Spengler, 2015; Vanni re et al., 2017b), and precondition the atmosphere for the development of consecutive low-pressure systems (Tilinina et al., 2018; Papritz et al., 2021; Vanni re et al., 2017a). In consequence, CAOs can regulate cyclone formation and strength and hence potentially affect downstream large-scale dynamics (Papritz and Grams, 2018). ~~However, the pathway of CAO influence on the upper-level flow is unclear.~~

Previous studies demonstrated that intense heat transfer in the regions of western boundary currents influences the position of the storm tracks (Kwon et al., 2010; Shaw et al., 2016) and plays an important role in the upper-level jet variability (Nakamura et al., 2008). In fact, Kwon et al. (2010) found in their modeling study that the absence of the Gulf Stream sea surface temperature (SST) gradient results in a reduced frequency of blocks downstream. Furthermore, O’Reilly et al. (2017) determined that wintertime poleward displacements of the jet stream are preceded by high eddy heat fluxes over the Gulf Stream and western North Atlantic. The mechanism behind those displacements is explained by Novak et al. (2015) and Kwon et al. (2020), who showed that the shift of the upper-level flow is caused by the northward shift of eddy heat flux in the lower troposphere. An increasing number of studies also indicate that the Gulf Stream region might serve as a moisture source for air masses ascending into the blocking regions. Yamamoto et al. (2021), using a 31-year climatology of backward air trajectories started from the upper-level North Atlantic-European blocks, found that the Atlantic basin provides most of the moisture for the moist air masses ascending into the block. Moreover, they established that trajectories that gather moisture from the ocean follow the path of the Gulf Stream and identified the region of the SST gradient in the western North Atlantic as the region where trajectories ascent to the upper troposphere. Those results are also in agreement with the findings of Pfahl et al. (2014), who determined that moisture supplies for WCBs are collocated with the regions of intense ocean evaporation in the western North Atlantic.

Throughout the literature, researchers have established the importance of ocean-atmosphere coupling over the Gulf Stream and its relevance for downstream large-scale dynamics (e.g. Vanni re et al., 2017b; Sheldon et al., 2017; Papritz and Spengler, 2015). However, the scientific community has yet to gain a clear understanding of the physical pathway through which signals from individual processes in the marine boundary layer are conveyed to the large-scale circulation (Czaja et al., 2019). In this study, we propose a possible explanation for this missing mechanistic link by conducting a case study of European Blocking from February 2019. This event brought record-breaking ~~heatwaves to western winter "heat" to Western~~ Europe and was accompanied by a series of upstream, rapidly intensifying cyclones. We ~~explore the relationship investigate the potential connections~~ between air-sea interactions over the Gulf Stream region and the formation of an upper-level ridge over western Europe ~~from both backward and forward Lagrangian perspectives using a Lagrangian perspective~~ in a synoptic study. ~~We structure the paper analysis. The paper is structured~~ as follows: First, we provide a detailed description of the data and methods,

including trajectory calculations (Section 2). Second, we introduce the European Blocking case study of February 2019 (Section 3.1). In the ~~following subsequent~~ section, we ~~describe in detail the results~~ provide a detailed description of our analysis ;
95 ~~which focuses on the connection between results, examining the characteristics of air masses that interact with the Gulf Stream and the development of an upper-level, quasi-persistent ridge assessing their links to cold air outbreaks and cyclones~~ (Section 3.2). Then, we analyze the moisture sources and transport paths of the air ascending into the block (Section 3.3), ~~and explain the variations of negative PV in the lower troposphere (Section A) and their possible relevance for blocking development~~. Finally, we ~~carry out a discussion of the results and draw final conclusions, synthesizing the results into a mechanistic link~~ discuss
100 our findings and establish a connection between air-sea interactions over the Gulf Stream, ~~the development of cyclones~~ cyclone development, and the ~~formation of the European Blocking event in February 2019.~~ potential influence of these air masses on atmospheric blocking events.

2 ~~Methodology~~ Methodology

2.1 Data

105 2.1.1 ERA5 reanalysis

The calculation of kinematic trajectories and the analyses presented in this study are based on the European Center for Medium-Range Weather Forecasts (ECMWF) reanalysis - ERA5 (Hersbach et al., 2020). For ~~the~~ most of the study, we use reanalysis data at the 3-hourly temporal resolution, interpolated on a $0.5^\circ \times 0.5^\circ$ horizontal grid. In addition, we employ ERA5 data with a higher temporal resolution of one hour for the investigation of cyclone tracks (Section 3), the vertical and horizontal distribution
110 of negative potential vorticity, potential temperature, and the cloud liquid water content (~~Section Appendix A~~). We chose the ~~lowest lower~~ 98 sigma-pressure vertical levels out of a total of 137 available levels for our investigation, covering the pressure range from ~ 26 hPa to the surface. The analyzed data covers the period from 10 to 28 February 2019.

2.1.2 Cyclone dataset

The cyclone tracks are obtained using the method of Sprenger (2017) and Wernli and Schwerz (2006), based on the identification and tracking of the sea level pressure (SLP) minima, defined as the grid points with SLP value lower than at
115 ~~the eight all the~~ neighboring grid points (eight in our case). In addition, the cyclone extent is determined by the outermost closed SLP contour surrounding the identified SLP ~~minima~~ minimum. This is limited to areas beyond 25° N/S, with a contour circumference cap at 7500 km. This approach ensures the exclusion of SLP minima linked to tropical convection and overly extensive cyclone masks that encompass multiple cyclones. The tracking algorithm is applied to hourly fields of SLP from
120 ERA5 reanalysis. Rapidly intensifying cyclones are identified using the criterion of Sanders and Gyakum (1980) of a central pressure drop of at least 24 hPa within 24 hours. ~~Complementary to the cyclone identification we use the surface sensible heat flux (SSHf) and the potential vorticity (PV) in the lowest model level to distinguish the cold sectors of the cyclones, following Vanni re et al. (2017a). In contrast to Vanni re et al. (2017a) we use a threshold of the SSHf higher than 0 W/m^2~~

and the PV lower than 0.1 PVU ($1 \text{ PVU} = 10^{-6} \text{ Kkg}^{-1} \text{ m}^2 \text{ s}^{-1}$). In their work Vanni re et al. (2017a) indicate that for some instances different thresholds can be more fitting. The thresholds of $\text{SSHF} > 0 \text{ W/m}^2$ and $\text{PV} < 0.1 \text{ PVU}$ were chosen based on the visual analysis of cold sectors' spatial distribution. This criterion is further normalized using the factor $\sin(60^\circ) / \sin \phi$, where ϕ represents the average latitude of the cyclone's center during the given time span.

2.1.3 Identification of the block and upper-troposphere negative potential vorticity anomalies.

The European Block in February 2019 is identified using the year-round weather regime definition of Grams et al. (2017) for the North Atlantic-European region. The ~~Block~~ block is characterized by a positive geopotential height anomaly over the eastern North Atlantic and Europe and a negative geopotential height anomaly upstream over Greenland. The methodology for identifying specific weather regimes is described in detail in Grams et al. (2017) and Hauser et al. (2022).

The formation of the atmospheric block in the Euro-Atlantic region is associated with the poleward advection of low PV air. The accumulation of low PV air in the upper troposphere leads to the development of negative potential vorticity anomalies (NPVA; Teubler and Riemer, 2016), which amplify the upper-level ridge. In our study, we use the method of Hauser et al. (2022) to identify NPVAs in the ERA5 dataset. First, the deviations of PV from a 30-day running mean climatology (1979-2019) centered on the day of interest are calculated. Then, vertical averages of obtained values between 500 and 150 hPa are computed and labeled as NPVA objects if they fall below the threshold of -0.8 PVU . In the next step, a quasi-Lagrangian framework is employed to follow the evolution of NPVAs and assign them to the lifecycle of the European Block in February 2019. PVAs are assigned to ~~active weather regimes~~ an active weather regime (European Block) based on their spatial overlap with a predefined regime mask. The mask is defined as the area where ~~weather regime pattern values are the vertical average PV anomaly of the composite for the respective weather regime is~~ below -0.3 PVU . ~~If a PVA overlaps with the mask by at least PVU. The composite is determined by averaging the PV between 500 and 150 hPa during the active phase of a weather regime (in our case European Block, as defined by Grams et al. (2017)). If there is at least a 10% overlap between a PVA and this mask during an active regime, it is attributed to phase, we associate it with that specific regime's life cycle. Sometimes, multiple PVAs may contribute to~~ Note that a single regime ~~.The weather regime PV pattern is the average of the low-frequency PVAs vertically averaged between 500 and 150 hPa during active days of the eye~~ can sometimes be influenced by several PVAs.

The formation of the studied block was related to one major NPVA ~~which formed 10 days prior to blocking onset~~, and another minor NPVA that ~~formed~~ appeared on 23 February over Greenland (Fig. ??2). The major NPVA ~~formed 10 days prior to blocking onset over~~ originated in the North Pacific and started to strengthen a few days before the block onset when it propagated into the North Atlantic. For the purpose of the present study, we neglect the NPVAs lifecycle prior to their arrival into the North Atlantic region.

2.1.4 Identification of cold air outbreaks

Cold air outbreaks (CAO) in the ERA5 dataset are identified using the method of Papritz et al. (2015). First, the air-sea potential temperature difference between $\theta_{\text{SST}} - \theta_{850}$ is calculated, where θ_{SST} denotes sea surface potential temperature and θ_{850} air potential temperature at 850 hPa. The reference pressure $p_0 = 1000 \text{ hPa}$ is used for the calculation of surface potential

Name of the dataset	Starting area	Duration of the trajectories	Characteristics
NPVA base trajectories	Upper troposphere NPVA.	-10 days	Started from the NPVA objects related to the European Blocking event in February 2019.
Subsets (NPVA base trajectories)			
NPVA no ascent trajectories	Upper troposphere NPVA.	-10 days	Trajectories that do not fulfill the ascent criterium of 500 hPa within 10 days backward.
NPVA trajectories			Ascent of 500 hPa within 10 days prior to the arrival in NPVA.
Subsets (NPVA trajectories)			
NPVA GS trajectories	Upper troposphere NPVA.	-10 days	Interact with the ABL over the Gulf Stream.
NPVA nonGS trajectories			Do not interact with the ABL over the Gulf Stream.

Table 1. Overview of the trajectory subsets used in the study. The ~~darker, bold rows indicate initial trajectory setups, while lightly shaded ones refer to data sets primarily used in the selection of trajectories based on their relation to the Gulf Stream (GS) mask or negative potential vorticity anomaly objects (NPVA) study are highlighted in bold font.~~ White rows refer to the further division of selected trajectories into different subsets and airstreams.

temperature. In agreement with Papritz et al. (2015), we require the $\theta_{SST} - \theta_{850}$ over the ocean to exceed 0 K to identify the CAO events.

160 To determine if a trajectory (Section 2.2) is a part of a CAO, we consider $\theta_{SST} - \theta$, where θ is the air parcel potential temperature (see Papritz and Spengler (2017)). If the potential temperature of an air parcel (at a pressure greater than 850 hPa) is lower than the SST beneath it, we classify the trajectory as a CAO trajectory.

2.2 Trajectory datasets

The LAGRANTO analysis tool (LAGRANTO Sprenger and Wernli, 2015) is employed to calculate kinematic trajectories, using three-dimensional wind on model levels from the ERA5 dataset described above. Output positions of trajectories are available in 3-hourly intervals and the following variables are traced along the trajectories: ~~temperature~~ pressure height (p), temperature (T), specific humidity (Q), potential vorticity (PV), potential temperature (θ), surface pressure (PS), ~~surface pressure, surface~~ latent heat flux (~~SLHF~~ SLHF), surface sensible heat flux (~~SSHFSHF~~ SSHFSHF), boundary layer height (BLH) and sea surface temperature (SST). ~~Two principal trajectory datasets are compiled, labeled according to the starting regions as NPVA and GS-SST. We have created a primary trajectory dataset, termed NPVA base trajectories (Tab.1). Those datasets are further divided into subsets that serve to illustrate the connections between the~~ This dataset is further filtered in order to work out the relationship between the atmospheric block and air-sea interactions over the Gulf Stream as well as the (GS), and to examine the specific properties of the trajectories. ~~All collections of trajectories are listed (Appendix A). The main trajectory subsets, which are crucial to this manuscript, are outlined in Tab.1 and are discussed below, relative fractions shown in Tab.2, and will be discussed in subsequent sections.~~

175 2.2.1 NPVA Trajectories

The ~~first principal base~~ trajectory dataset comprises 10-day backward trajectories started from the upper-level NPVA objects (Section 2.1.3) every 3 hours between 20 February 09:00 UTC and 28 February 12:00. ~~The 00 UTC (NPVA base trajectories, Tab.1). Those~~ 10-day kinematic backward trajectories are initiated from ~~an equidistant grid of $\Delta x=100$ km and~~

~~$\Delta y=25$ hPa vertically between equidistant grid points of size 100x100 km. Vertically, the starting points span from 500 and to 150 hPa within both NPVAs (Fig. ??, Section 2.1.3), with an interval of $\Delta p=25$ hPa. To avoid the possibility of trajectory double-counting, we remove those that remain for two consecutive time steps within the starting grid of the NPVA. This filtering technique removes approximately 10% of trajectories, ensuring that we do not count the same air mass multiple times.~~

In the consecutive analysis, the obtained trajectory dataset is refined as we apply additional ~~filtering and~~ selection criteria. ~~First, to~~ To select only the ascending trajectories, we require trajectories to experience a pressure decrease of 500 hPa within 10 days prior to the arrival in the upper-level NPVA, hence the air parcel can ascend at any time and any rate ~~-(NPVA trajectories, Tab.1)~~. The threshold of 500 hPa is chosen to ensure that the trajectory has ascended all the way from the lower troposphere ~~and is motivated by common criteria to identify WCB air streams (e.g. Madonna et al., 2014). However, it is a bit weaker and allows ascending motion over a longer time span~~ enabling the analysis of ocean influence on the ascending air ~~Approximately 53~~ also independent of WCB activity. Approximately 43% of the ~~trajectories in the initial dataset-NPVA base trajectories~~ experience such an ascent of 500 hPa before their arrival into the upper-level NPVA. ~~Second, to avoid the possibility of trajectory double-counting, we detect those that remain for two consecutive time steps within the starting grid of the NPVA and remove them from the dataset. This filtering technique removes approximately 10% of trajectories. The remaining trajectories-Those ascending and filtered trajectories~~ will be referred to throughout the following analysis as ‘NPVA trajectories’ (Tab.1).

~~For the ascending NPVA trajectories and their subsets (NPVA GS and NPVA nonGS) we further refer to their inflow, ascent, and outflow stages. Therefore at a given time, we identify the position of air parcels from all trajectories with different trajectory starting times and group them in an inflow ($p > 800$ hPa), ascent ($800 \leq p < 400$ hPa), and outflow ($p < 400$ hPa) layer. The boundaries of layers are motivated by similar layers used for classifying WCB air streams (e.g. Binder et al., 2020).~~

2.2.2 NPVA GS Trajectories

Taking into account the importance of the Gulf Stream for the selected study, we create an additional subset of trajectories consisting of only those NPVA trajectories that have passed over the Gulf Stream in the lower troposphere. We define the boundary for the lower troposphere ~~as at 800 hPa, hPa, which is~~ commonly used as an upper ~~limit of the WCB inflow boundary of the layer in which the ascending WCB air stream has its inflow and gains moisture~~ (e.g. Binder et al., 2020). The region of the Gulf Stream (GS masks) is defined for every 3-hourly timestep of the ERA5 dataset for February 2019 using the following steps: (i) first, the horizontal gradient of the SST is identified in both west-east and north-south directions, (ii) a threshold of $|\nabla SST| > 2K$ is applied to extract the area of the Gulf Stream SST front, (iii) a buffer of 100 km is added to the identified gradient, creating a continuous region.

In the following, we refer to those trajectories as ‘NPVA GS trajectories’ (Tab.1). The rest of the trajectories, i.e. those that did not interact with the ABL over the Gulf Stream, are labeled as ‘NPVA nonGS trajectories’ ~~and~~

2.2.3 GS Trajectories

The second principal dataset consists of trajectories that are started from the lower troposphere over the region of the Gulf Stream, defined using the same masks as for the selection of NPVA-GS trajectories (see Section 2.2.2). Those trajectories are run both backward and forward in time for 10 days, in total having a duration of 20 days with time 0 indicating their location over the Gulf Stream SST front region. The spatial resolution of the equidistant starting grid is $\Delta x=50$ km in the horizontal and $\Delta y=25$ hPa in the vertical ranging from 700 to 1000 hPa. Similar to the previous setup, only those trajectories that experience a change of pressure of 500 hPa within 10 days from the start forward in time are selected. This criterion is applied as the goal of the study is to establish the connection between air-sea interactions over the Gulf Stream and upper troposphere dynamics. Approximately 43% of trajectories of the original dataset meet this criterion. Furthermore, to avoid double-counting, a filtering criterion is applied to eliminate trajectories remaining within the starting region for the first two time steps, leading to the reduction of the total number of trajectories by $\sim 15\%$. The acquired dataset is labeled as ‘GS trajectories’ (Tab.1).

2.2.3 GS NPVA Trajectories

For each trajectory within the NPVA GS and NPVA nonGS datasets, we pinpoint the onset of ascent. This specific moment is identified when the trajectory’s pressure first drops below 800 hPa. After this, the trajectory consistently rises until it reaches the upper troposphere, marked by pressures falling below 500 hPa.

In a similar manner as in the case of NPVA-GS trajectories, we select a subset of the GS trajectories, that at some point within 10 days from leaving the Gulf Stream region end up in the NPVAs (Section 2.1.3) associated with the analyzed European Block (GS-NPVA trajectories, Tab. 1).

2.2.3 Further trajectory subsets

In each collection of the NPVA and GS trajectories we additionally identify the following air streams (Tab. 1):

- CAO – to determine if a trajectory is a part of a CAO, we consider $\theta_{GST} - \theta$, where θ is the air parcel potential temperature (see Papritz and Spengler (2017)). We use two different thresholds to identify CAOs, 0 K (CAO1) and 2K (CAO2), to distinguish between weaker and stronger CAOs.
- DH – trajectories that experienced diabatic heating of $\Delta\theta \geq 2$ K within 3 days before their arrival in the block, following Pfahl et al. (2015).
- WCB – trajectories fulfilling the warm conveyor belt criterion of 600 hPa ascent within 48h or less in, line with Madonna et al. (2014), in any time window within the 10 days backward calculation for NPVA trajectories and 10 days backward/forward for GS trajectories, with the additional rule for GS trajectories that the WCB ascent has to end within the forward part of the trajectory.
- DI – trajectories fulfilling the dry intrusion criterion of 400 hPa descent within 48h following the definition of Raveh-Rubin (2017), in any time window within the 10 days backward calculation for NPVA trajectories and 10 days forward/backward for

~~GS trajectories, with the additional rule for GS trajectories that the dry intrusion's descent has to start in the upper troposphere before the air parcel reaches the Gulf Stream.~~

2.3 Moisture source identification

245 The method of Sodemann et al. (2008) is applied for the purpose of moisture source identification. In this approach, a specific humidity change along a trajectory is considered as an uptake if the specific humidity difference between two-time steps (difference of 3 h) exceeds 0.02 g/kg. Each uptake is given a weight based on all consecutive changes in the specific humidity along the trajectory. This means that the contribution of each uptake is adjusted by considering precipitation events en route and subsequent uptakes. This method has been widely recognized as appropriate for the identification of moisture sources and
250 used in a number of other studies (e.g. Papritz et al., 2021; Xin et al., 2022; Jullien et al., 2020; Aemisegger and Papritz, 2018).

This method is applied to both the NPVA GS and the NPVA nonGS trajectories to identify the sources of moisture present at the start of the ascent. The use of the start of the trajectory's ascent as a reference time for the moisture diagnostic allows us to identify the sources of moisture contributing to latent heat release during an air parcel's upward movement. For the purpose of this analysis, every backward NPVA trajectory (NPVA GS and NPVA nonGS, Tab.1) is extended another 10 days backward
255 from the time when the ascent started.

3 Results

3.1 The European Blocking Heatwave 2019

The European Blocking event in February 2019 lasted for about 7 days, from 20 to 27 February. The duration of this event was below the average for winter block events in the Northern Hemisphere (Wazneh et al., 2021). However, it was accompanied by
260 record high temperatures for this month in France, the Netherlands, and the United Kingdom (Young and Galvin, 2020) with 2 m temperature anomalies in western Europe exceeding +10 °C (Fig.??1). This exceptional, wintertime heatwave was linked to the formation of a quasi-stationary ~~r~~-upper-level ridge, which brought southerly airflow and clear skies to western Europe (Leach et al., 2021).

Temperature data from weather stations illustrate the extreme nature of this event. The highest temperature anomalies were
265 observed on 26 and 27 February (Fig.??, h1d), with the record high temperature in February for the United Kingdom of 21.2°C measured in Kew Gardens, London (Young and Galvin, 2020). Record-breaking observations were also made in Scotland (18.3°C), the Netherlands (18.9°C), and Sweden (16.7°C), highlighting the spatial extent of the event (Young and Galvin, 2020).

In the following, we discuss the synoptic evolution based on maps of potential vorticity at 315 K and mean sea level pressure
270 Fig.2. In addition, the tracks of all cyclones during the study period are shown in p Fig. 3. Europe has already experienced moderate winter weather prior to the blocking event. In the second part of February, the upper-level flow was repeatedly interrupted by the formation of upper-tropospheric NPVAs. Two days prior to the analyzed event, on 18 February, the west-

to-east propagation of the jet stream was disrupted by the NPVA in the upper troposphere stretching over western Europe and another over the central North Atlantic (white, dashed contours in Fig.??2a). ~~The resulting anticyclonic circulation Over Europe, this~~ was accompanied by south and southwesterly flow ~~bringing warm temperatures to in the western part of the anticyclone bringing high temperatures to western and~~ central Europe with anomalies exceeding 10°C (Fig.??1a). On 18 February, the NPVA GS trajectories were found to be in their ascent phase, distinctly spread over the western North Atlantic, as shown by the red crosses in Fig.2a. Yet, the bulk of air parcels that later ascend into the blocking region remained in the lower troposphere. These air parcels were predominantly observed in regions influenced by CAOs in the western and central parts of the North Atlantic (green crosses in Fig.2b). Those CAOs occurred behind the very intensive cyclone L0 (Fig.3a) and ahead of another potent cyclone, L1, emerging near the North American coastline (Fig. 3a). Three days later, the upper-level flow was disturbed by another major NPVA, extending from southern Europe to the North Atlantic and Greenland (~~grey magenta~~ shading in Fig.??2c). In contrast to the NPVA object from 18 February, this new NPVA became quasi-stationary and persisted over the region for a week. ~~Clear skies and~~ Air parcels in their outflow stage and initially emerging from the Gulf Stream, encompass a notable segment of this major NPVA (black crosses, Fig.2c). In addition, a considerable number of these parcels are in the ascent stage (red crosses, Fig.2c), progressing towards the upper-level ridge. Both the outflow and ascent are potentially linked to the ~~continued inflow of warm air associated with the anticyclonic circulation (Leach et al., 2021) further intensified the warm spell over France, the Netherlands, and the United Kingdom (Fig.??d, f).~~ On 23 February, ascending air stream of the upper-level flow was further disturbed by another minor NPVA (light blue in Fig.??e), which strengthened the block and lead to its extension westward. 27 February marks the last day of the blocking event when both the major and minor NPVAs started to shrink in size and propagated east (Fig.??g).

The close succession of cyclones over the North Atlantic in the second part of February 2019 disrupted the normal progression of weather systems in the North Atlantic-European region. Both before the onset and during the blocking event, several rapidly intensifying cyclones and smaller low-pressure systems developed over the ocean rapidly intensifying cyclone L1 (Fig.??). Prior to the formation of the block, a rapidly intensifying cyclone (LE0, Fig.??a and blue line in ??a) led to the expansion of an upper-level ridge. This low-pressure system initiated the sequence of the cyclones that played an important role in the present case study. Moreover, it triggered an intense CAO and strong surface evaporation events 3a), followed by a smaller cyclogenesis (11.1, 11.2) in its wake. The transit of this cyclone, characterized by a pressure drop of 39 hPa within 24 h, resulted in the development of a CAO over the western North Atlantic (Fig.??a). The second rapidly intensifying cyclone developed on 18 February (LE1, Fig.??e, light blue line and central North Atlantic, as seen in Fig.??a) over the Gulf Stream region and crossed the North Atlantic toward the southern tip of Greenland. The pressure drop during its intensification phase reached 39 hPa within 24h. Moreover, the divergent outflow caused by the WCB of this cyclone modified the 2d. This is where the majority of trajectories in the inflow stage (green crosses) are positioned at that moment. On 23 February, the upper-level NPVA (~~black crosses~~ flow was further disturbed by another minor NPVA (light green in Fig.??e), leading to its growth in size. In the lower troposphere, 2e), which strengthened the block and led to its extension westward. This, combined with clear skies and the sustained influx of warm air due to the anticyclonic circulation (Leach et al., 2021), amplified the warm spell across France, the Netherlands, the passage of this cyclone resulted in a strong CAO event over the Gulf Stream region (Fig.??b).

The northward progression of the LE1 cyclone on 21 February was followed by the development of several secondary, much weaker cyclones in the central North Atlantic (L1, L2, Fig.??b). Despite their weakness, they acted to maintain the advection of cold air across the ocean (Fig.??b) and reinforce the upper-level NPVA (United Kingdom, and even Scandinavia (Fig.1c). Examining Fig.2e,f, we see distinct patterns. The green crosses in Fig.2f represent trajectories at the inflow stage, while the red and black crosses in Fig.??e) through cross-isentropic ascent.

The third rapidly intensifying cyclone emerged on 21 February (LE2, green line in Fig. ??e, ??a) and followed a similar path as the one from 18 February. The highest pressure drop observed for this system was 25 hPa within 24 h. The latent heat release in the ascending air stream of this cyclone led to the formation of 2e correspond to the ascent and outflow stages, respectively. These patterns collectively display a WCB-like structure, directly associated with cyclone L2. This structure not only suggests the genesis of a minor NPVA (Section 2.1.3, blue shading in Fig. ??e) that later joined the main NPVA (Fig. ??g) and reinforces but also, as indicated by the presence of black crosses in the major NPVA, underscores their potential role in sustaining the block. It is important to highlight the fact that cyclone LE2-L2 propagated into the region of high surface fluxes, related to CAOs, left behind by cyclone LE1-L1 (Fig.??b2d). Furthermore, the advection of cold air behind the cold front of LE2-L2 resulted in another strong surface evaporation event over the Gulf Stream region (Fig.??e).

The last rapidly intensifying cyclone had genesis on 26 February (LE3, purple line in Fig.??g, ??a2f). 27 February marks the last day of the blocking event when the NPVA started to shrink in size and propagate east (Fig.2g) and temperature anomalies in western Europe reached their peak (Fig.1d). Air parcels originating from trajectories that interacted with the Gulf Stream are predominantly found in the upper troposphere, in the region covered by the NPVA, or in its vicinity (black crosses, Fig.2g). The strengthened outflow associated with ascent of those air parcels was most probably associated with cyclones L3 and L4 (Fig.3). Unlike cyclones L1 and L2, the tracks of cyclones L3 and L4 are predominantly constrained to the western North Atlantic. The enhanced outflow from the rising air streams of these cyclones could have played a role in fortifying the cyclone's ascending air stream may have contributed to reinforcing the upper-level NPVA from western direction (gray a westerly direction, as indicated by the magenta shading and black crosses in Fig.??g). Similar to the previously described low-pressure systems, it also caused a CAO event 2g. Following the passage of cyclone L3, a subsequent CAO event was observed over the Gulf Stream (Fig.??e). The 2h). However, unlike earlier events, this CAO was more spatially confined, largely limited to areas near the Gulf Stream.

It should be emphasized that extreme cyclones of 15, 18, 21, and 26 February were accompanied by weaker low-pressure systems developing in the central part of the North Atlantic (L1-L5, Fig.??b). Their development light blue lines in Fig.3), bringing the overall count to almost 20 cyclones in the North Atlantic either preceding or concurrent with the blocking event. The evolution of these systems led to the expansion of CAOs further into the ocean and the widespread occurrence of strong spread of CAOs deeper into the North Atlantic Ocean, resulting in a pervasive presence of intense upward surface fluxes in the area (Fig.??region (not shown).

This synoptic overview suggests that a series of factors contributed to the creation Our synoptic analysis points to a combination of factors that led to the formation of the block in February 2019 and the resulting observed record-high temperatures. The cyclones set the stage for trajectories from the Gulf Stream to move into the upper troposphere. These same

	heightWCB (%)	DI(%)	CAO (%)	DI-CAO-DH (%)	DH(%)	$\Delta\theta K$ (0-3 days)	Δt of ascent to strongest uptake	Fraction of ascending trajectories (%)	Fraction of all (%)
NPVA GS trajectories	31.2	11.4	82.0	9.11	98	20.77	86	28	12
NPVA nonGS trajectories	29.7	3.71	40.8	2.1	54.7	13.88	67	72	31
NPVA trajectories	29.8	5.99	52	4.24	63.25	16.51	76	100	43
NPVA non ascent trajectories	0	0.67	2.4	0.01	38	8.36	-	0	57
NPVA base trajectories	11.87	2.8	22.3	1.8	48.17	12.66	76	43	100

Table 2. Fractions of various air streams within the NPVA trajectories and the subsets created for the analysis presented in the article. WCB, DI, CAO, DI-CAO-DH, and DH, refer to proportion within their own subset. For NPVA GS, NPVA nonGS, and NPVA trajectories 'Fraction of ascending trajectories' refers to the proportion within NPVA trajectories, which are all ascending. 'Fraction of all' denotes the proportion within the entire set of NPVA base trajectories. $\Delta\theta K$ (0-3 days) refers to the change of potential temperature (θ) within 3 days from the start of the trajectories (Pfahl et al., 2015). Δt of ascent to strongest uptake refers to the average time delay between the strongest uptake of trajectories and the time they start ascending later. See Section 3.2 for more details.

345 cyclones also triggered distinct CAOs in the inflow areas of the trajectories, leading to increased heating and moistening of the atmospheric boundary layer. In the following sections, we will study in detail the importance of the described cyclones and CAO events for the development of the atmospheric block in February 2019. examine the details of NPVA GS trajectories to better understand the evolution of the air masses that interacted with the Gulf Stream.

3.2 Connection between the Gulf Stream region and the large scale dynamics

To investigate a potential link between the Gulf Stream region and the upper-level circulation during the blocking episode, we investigate the characteristics of the two main sets of trajectories (Section 2.2). Figure 4 shows properties of the air parcels that start from the upper-level NPVA objects (NPVA trajectories, Tab.1, Fig. ??a) and from the Gulf Stream (GS trajectories, Tab. 1, Fig. ??, b). Note that the times in Fig. ?? refer to backward trajectories started in the NPVA objects forming the block in February 2019 (Section 2.2). Given our study's aim to understand how the Gulf Stream influences the upper troposphere, we mainly focus on trajectories that show an ascent of 500 hPa within 10 days backward and that traveled over the time when the trajectories are started in the NPVA objects and the Gulf Stream, respectively. As stated in Section 2.2, these trajectories ascend by at least 500 hPa prior to arriving in the NPVA objects (for NPVA trajectories) and after starting from the GS region (for GS trajectories). Those base sets represent 53% of all trajectories started from NPVA objects (NPVA trajectories) and in the lower atmosphere (referred to as NPVA GS trajectories in Tab.1). Out of all the NPVA base trajectories (Tab.1), 43% of all trajectories started from the GS region (GS trajectories).

360 First, we determined the fraction of NPVA trajectories passing over the Gulf Stream in the lower troposphere (NPVA GS trajectories, Tab.1) and of the GS trajectories ending up in the NPVAs in the upper troposphere (GS NPVA meet the ascent criteria, and 28% of those are classified as NPVA GS trajectories, Tab.1). On average, more than 23% of the NPVA trajectories interact with the ABL (Tab.2). Although NPVA GS trajectories represent just 12% of all trajectories originating from NPVAs (NPVA base trajectories), a focus on these helps to better understand how signals from air-sea interactions over the Gulf Stream region (black, dashed line in Fig. ??a) and 61% of the GS trajectories travel into the NPVAs forming the block (black, dashed line in Fig. ??b). A more detailed analysis of the temporal evolution reveals that the fraction of the propagate to the upper

troposphere. Furthermore, as will be shown in the following, their distinct properties hint at a disproportional relevance for the formation and maintenance of the atmospheric block.

370 First, we examine the differences in pressure changes between NPVA GS and nonGS trajectories. NPVA GS trajectories changes only by a maximum of $\pm 10\%$ throughout the lifecycle of the block and does not fall below 18% , nor exceed 40% (Fig.?? initially undergo a slight descent from the mid-troposphere towards the atmospheric boundary layer (green shading, Fig.4a). More variations are found in the fraction of the GS NPVA trajectories within all ascending GS trajectories (black, dashed line in Fig. ??b). 10 days prior to the onset of the block, 30% of GS trajectories travel into the upper-level NPVA. In the following days, as we get closer to the blocking event, this fraction increases to 90% on 18 February. The increases in the fraction of trajectories ending up in the upper-level block are related to the development of cyclones, first from 13
375 February (LE0) and later the one forming on 18 (LE1). Here, on average, they remain for about 48-72 hours. Then, quite swiftly between -72 h to -36 h, they ascend into the upper troposphere. Conversely, on average NPVA nonGS trajectories start from higher pressure levels, and ascend steadily to the upper troposphere (blue shading, Fig.??a) and 21 of February (LE2, Fig. ??a). Once we get closer to the end of the blocking event the number of the GS NPVA trajectories starts to decrease. This decline coincides with the shrinking of the upper-level NPVA and its eastward propagation. On 28 February, only $\sim 20\%$ of the
380 GS NPVA trajectories ascend into the blocking region (Fig.4a). The ascent of NPVA GS trajectories closely mirrors the distinctive features of the warm conveyor belt (WCB), which typically occurs in the warm sector of extratropical cyclones. As defined by Madonna et al. (2014), a trajectory is denoted as a WCB trajectory if it experiences an ascent of at least 600 hPa within a 48-hour interval. It is crucial to note that their criterion focuses only on the most vigorous part of the air stream that ascends in the warm sector of an extratropical cyclone. Indeed, about 87% of NPVA GS trajectories ascend from pressures greater than
385 800 hPa to pressures below 500 hPa within only 48 hours, reflecting their relatively fast ascent. Meanwhile, when applying this criterion to NPVA nonGS trajectories, only 72% of them meet the condition.

In the next step of our study, we focus in more detail on the airstream characteristics of the NPVA GS trajectories and the GS NPVA trajectories (Tab.1). This analysis is carried out by dividing the trajectories into different airstreams: CAO, WCB, DI, and DH (Section ??; Tab.1). As previously described in Section 3.1 the development of multiple cyclones over the Gulf Stream
390 region throughout the second part of February 2019 provided conditions favorable for the advection of cold air from higher latitudes across the warm waters of the western North Atlantic, particularly south of the Gulf Stream (Fig.??). Trajectories passing through the Gulf Stream region often coincide with a CAO event, as shown by the high percentage of CAO trajectories in both NPVA GS and GS NPVA trajectories, which were approximately 67% and 89% , respectively. To gain further insight, we divided the CAO trajectories into subsets based on their strength, distinguishing between very weak (blue in Fig.??) and
395 stronger (teal in Fig.??) characteristics (see Section ??). It's worth noting that the percentage values mentioned refer specifically to the strong CAO subsets. Furthermore, the fraction of CAO trajectories in both subsets remained high throughout the case study, indicating that CAO events were prevalent in the western North Atlantic in February 2019. CAOs lead to a large exchange of heat and moisture between the ocean and atmosphere, warming and moistening the air parcels. Consequently, almost all of the NPVA GS and GS NPVA trajectories that interacted with or were started from the Gulf Stream are diabatically heated by at
400 least 2 Applying the strict WCB requirement of 600 K (orange in Fig. ??). Steinfeld and Pfahl (2019) found in their hPa ascent

within a 48, both NPVA GS and nonGS trajectories comprise approximately 30% of WCB trajectories (Tab.2). The temporal variations of PV for NPVA GS trajectories, as shown in Fig.4e, display a typical WCB-like behavior. An initial increase in PV from -72 to -48 h followed by a decrease, suggests the release of latent heat due to condensation in WCB-like ascent (Madonna et al., 2014). Indeed the average potential temperature increases from 294 K to 315 K in this time window along with a marked moisture reduction (Fig.4f). Thus the formation of stratiform and convective clouds, as well as precipitation, leads to the release of latent heat, resulting in diabatic heating of rising air masses. The influence of diabatic heating on blocks within the North Atlantic-European region has been underscored by recent research (e.g. Steinfeld and Pfahl, 2019; Steinfeld et al., 2020; Pfahl et al., 2019). Within a 38-year global analysis of backward trajectories started in the study, Steinfeld and Pfahl (2019) identified that between 30-45% of trajectories initiated in upper-level blocks that the fraction of diabatically heated trajectories exceeds 30-45%, in contrast to a larger fraction obtained by Yamamoto et al. (2021) ~51.8%, who attributed the higher values to the use of different ~~underwent~~ diabatic heating. This contrasts slightly with the 51.8% reported by Yamamoto et al. (2021), who suggest that variations in blocking definitions and trajectory setup. When considering all NPVA trajectories released from the upper level NPVA objects after initial filtering (Section 2), we found, for this particular case, that ~49% of them have experienced diabatic heating approaches could account for the difference. For a quantitative comparison with these studies, we detect diabatic heating in trajectories based on the criterion set by Pfahl et al. (2015), which specifies a change in potential temperature ($\Delta\theta$) of at least 2 K over a 3-day period from the onset of backward trajectories. Our findings indicate that approximately 48% of all trajectories started from the NPVA objects (NPVA base trajectories, see *DH* Tab.2) underwent diabatic heating in the 3 days prior to the leading up to their arrival in the blocking region. Moreover, when considering NPVA GS and NPVA nonGS datasets together, therefore after the application of the ascent criterion, this number increases to ~63%. This observation aligns with the aforementioned data from previous climatological investigations (Steinfeld and Pfahl, 2019). As anticipated, a larger proportion of ascending trajectories, 63%. Such a large fraction of trajectories undergoing diabatic heating, similar to those obtained in both climatological studies, demonstrates the importance of diabatic processes and their potential role in the development of European Blocking in February 2019.

Next, we consider the trajectories that experience rapid ascent into the upper troposphere of 600 hPa within 48 h (green in Fig.??; Madonna et al., 2019). On average 24% of the GS and 30% of the NPVA trajectories are classified as WCB trajectories. A closer look at the temporal evolution of %, undergo diabatic heating compared to just 38% of non-ascending trajectories. This contrast is further amplified when distinguishing between GS and nonGS trajectories within the ascending category, with rates of 98% and 54.7%, respectively. The dominance of diabatic heating in the air masses that interacted with the Gulf Stream is further mirrored by an increase in potential temperature visible in Fig.4b, where NPVA GS trajectories demonstrate on average 21 K rise, which is 7 K more than that in nonGS trajectories (Tab.2). Building on the insights of Steinfeld and Pfahl (2019); Pfahl et al. (2015), such pronounced diabatic heating, often termed 'latent heating bursts', suggests an interplay between the WCB fractions reveals that for the NPVA trajectories, the percentage of WCB trajectories remains higher than 20% for the whole duration of the block and between 22-23 February it exceeds 40%, whereas temporal variations in the proportion of the GS WCB NPVA trajectories (green in Fig.??b; Tab.1) shows more fluctuation. Moreover, there appears to be a connection between the increases

435 in the fraction of WCB trajectories and the growing number of trajectories defined as GS CAO NPVA (blue and teal preceding
cyclones.

Strong heating occurs also at the surface, as indicated by negative values in the sensible and latent heat fluxes (Fig.4c,d).
This heating correlates with the prevalent CAO events across the western and central North Atlantic, as shown in Fig.??b; Tab.
1).

440 A significant portion of the NPVA GS and GS NPVA trajectories undergoes rapid descent of 400 hPa within 48 hours,
satisfying the criterion for dry intrusions (violet in Fig.??; Raveh-Rubin, 2017). Dry intrusions are associated with exceptionally
strong surface sensible and latent heat fluxes, resulting in moistening of air parcels before they ascend again into the upper
troposphere. The examination of 2. Supporting this, a considerable portion (82%) of NPVA GS trajectories are identified as
CAO (Tab.2, see Section 2.1.4), in agreement with the findings presented in Section 3.1. The development of multiple cyclones
445 in the western North Atlantic created conditions favorable for the spatial distribution of detected DIs, for both the NPVA GS and
the GS NPVA trajectories, revealed that dry, cold air descending from the upper troposphere interacts with the boundary layer
mostly in the confined region northeast of the Florida peninsula, over the southern section advection of cold air of continental
origin over warmer waters, particularly south of the Gulf Stream. This region stands out in the analysis of moisture sources
for the GS trajectories presented in the next section (Fig.??e, Section 3.3) resulted in enhanced heat and moisture exchanges
450 between the ocean and atmosphere, even leading to the emergence of negative potential vorticity values, signaling an unstable
environment (see Appendix A).

The fractions of each of the analyzed air streams, with an exception of DH, change slightly throughout the studied period
(Fig.??). Those temporal variations are less pronounced for the NPVA trajectories, compared to the GS ones. Overall, such
fluctuations in the number of trajectories identified as CAO, WCB, or DI (Fig.??) are related to the formation and intensity of
455 extratropical cyclones developing in the northwestern North Atlantic. The rapid intensification of cyclones (Fig.??a, LE0-LE3)
tends to be associated with higher fractions of WCB airstreams (Fig.??; Binder et al., 2016). For instance, Importantly, some
CAO events coincided with ‘dry intrusions’ (DIs), defined by Raveh-Rubin (2017) as the descent of 400 hPa within 48 h.
DIs are the increases in the fraction of WCB trajectories around 23 February for the descending counterpart to WCBs and
typically occur in the cold sector of extratropical cyclones (Raveh-Rubin, 2017). When DIs reach the lower troposphere
460 they affect the atmospheric boundary layer through enhanced surface fluxes, heightened wind speeds, and the elevation of
the planetary boundary layer (cf. Ilotoviz et al., 2021). Thus it is worthwhile investigating if NPVA trajectories also feature
characteristics of DIs. We find 11.4% of the NPVA GS trajectories and 21 February for the GS NPVA trajectories are related to
the rapidly intensifying cyclones from 18 (LE1) and 21 February (LE2, Fig.??a). The match between the fractions of the CAO
and WCB trajectories (Fig.??b) found for the GS NPVA trajectories indicates that there is a potential link between intense
465 ocean evaporation events and the development of the WCB. Similar observations have already been reported in several studies
(e.g. Aemisegger and Papritz, 2018; Pfahl et al., 2014; Eckhardt et al., 2004). The relatively high number of DI trajectories on
21 and 22 February for the NPVA GS trajectories and on 14 to 17 February for the GS NPVA trajectories indicates that those
DIs might have provided conditions that favored the formation of the rapidly intensifying cyclones developing on 18 and 21
February (Fig.??a; Raveh-Rubin, 2017) featuring DI characteristics, Tab.2). DIs occurred particularly over the southern part of

470 the Gulf Stream, northeast of Florida (not shown). The extreme nature of dry intrusions and their role in potentially triggering
intense CAO events prompted us to analyze trajectories that sequentially experience DI, CAO, and diabatic heating (DH).
Notably, a majority of DI trajectories follow this sequence (~80%, cf. Tab.2). Thus, in our case study a DI in the vicinity of the
GS has a very high likelihood of later ascent in a WCB-like air stream into the upper troposphere and contribute to blocking.
475 While these trajectories represent a minor portion of all those originating from NPVAs (~2%), we find this dynamical relevance
of DI air streams interacting with the Gulf Stream noteworthy and of potential relevance for subsequent research studies.

~~The previously described results suggest a strong connection between the CAO-induced air-sea interactions over the Gulf Stream and the large-scale dynamics associated with the formation of the block in February 2019. While~~
~~Our findings emphasize that while only 28% of all ascending trajectories originate from the block and interact with the Gulf Stream in the lower~~
~~troposphere, these trajectories display unique features, suggesting pronounced block-cyclone interactions. In addition, while it~~
480 is widely established that diabatic heating in regions of intense surface heat fluxes influences the large-scale atmospheric circu-
lation (e.g., Pfahl et al., 2015; Yamamoto et al., 2021; Tilinina et al., 2018), the understanding of the mechanistic link between
processes that take place within the cold sectors of CAOs in the wake of extratropical cyclones and upper-level ridge formation
is still missing (Czaja et al., 2019). Our results show that the intense, CAO-induced air-sea interactions in the western North
Atlantic and an episode of European Blocking might be inherently linked. Furthermore, the connection between the surface
485 fluxes and coherent air streams hints at a dynamical linkage of the Gulf Stream front to the large-scale atmospheric circulation.
In the following section, we aim to further detail this mechanistic link.

3.3 Moisture sources for NPVA ~~GS~~ trajectories

The rapid, cross-isentropic ascent of air parcels into the upper-level NPVA is driven by the latent heat release during cloud formation and precipitation (Joos and Wernli, 2012). For clouds and precipitation to form, a sufficient moisture supply is
490 needed (Eckhardt et al., 2004; Pfahl et al., 2014). ~~Using the method of (Sodemann et al., 2008) we analyzed the sources of~~
~~moisture~~ Employing the method from (Sodemann et al., 2008), we examined the moisture sources for the ascent of ~~the NPVA~~
~~GS trajectories, and for those that did not directly interact within the Gulf Stream region in the lower troposphere—labeled as~~
both NPVA GS and NPVA nonGS trajectories (Tab.1, Section ??). However, given our paper's primary focus, we primarily
concentrate on trajectories that interacted with the Gulf Stream.

495 ~~We will first~~ First, we will focus on the timing and spatial distribution of moisture uptakes of the trajectories. NPVA GS
trajectories ~~(see Table 1). On average, these trajectories gain moisture about~~, on average, accumulate moisture around 3.5 days
prior to their ascent, as indicated by the orange bars in Figure ??a and Table 2. ~~Approximately before their ascent (Tab.3).~~
Roughly 78% of moisture uptakes take place within the first seven days prior to this moisture is gathered within the seven
days leading up to the ascent, with the largest contributions found within the first five days most significant portion (about
500 60%, indicated by the orange line in Figure ??a and Table 2). For many trajectories, moisture is supplied shortly (24 hours)
acquired in the first five days. In comparison, NPVA nonGS trajectories start collecting moisture about 3.8 days prior to ascent
, as shown by the orange bars in Figure ??a. Over the course (Tab.3), with 67% of uptakes taking place within the initial week
and 48% within the first five days backward. Interestingly, over a span of 10 days, 75% of the uptakes take place only 44% of

NPVA nonGS trajectories occur over the ocean and 25% over land, as detailed in Table 2. On average, in contrast to 78% for NPVA GS trajectories take 2.6 days (Tab.3).

Furthermore, from the start of ascent to arrive in their ascent, NPVA GS trajectories reach the upper-level NPVA, as indicated by the orange bars in Figure ??b and Table 2. These results indicate that moisture uptake for air parcels passing over the Gulf Stream, subsequent ascent, and arrival in the upper-level NPVA occur in rapid succession in an average of 2.6 days (Tab.3). This is notably quicker than the 6.65 days taken by NPVA nonGS trajectories, implying that the ascent regions for these two trajectories might be distinct.

The Figure 5c illustrates the spatial distribution of moisture uptakes for the all NPVA GS trajectories is presented in Figure ??c. The highest frequency of moisture uptakes for NPVA GS trajectories is found in the region of the . There are two prominent areas of moisture uptake: one close to the Gulf Stream and in another over the central North Atlantic. Figure ??a and b indicates that moistening and heating of air masses in this stretch of the ocean are related to the air-sea interactions taking place during CAOs—triggered by the passing, rapidly intensifying cyclones. Interestingly, these regions seem to align with the locations of CAOs observed during our study period (Fig. ??a; Fig. ??).

The method for moisture source identification used in our analysis enables the calculation of moisture uptakes contribution from each source area (5a). This may suggest that CAOs, and resulting upward latent heat fluxes (Fig.5b), might play a role in the water cycle of NPVA GS trajectories. Examining the specifics of these uptake regions further underscores the significance of certain geographic locations in the moisture collection process. Our moisture source identification methodology indicates that the majority of the moisture originates from regions relatively close to the block (Fig. ??5e). It is noteworthy that, despite the backward extension of trajectories used to identify moisture sources, the majority of uptakes occurred quite close to the region of the block. Moreover, moisture sources. In particular, 80-90% of the uptakes come directly from the area of the Gulf Stream accounted for 80-90% of the uptakes, together with the uptakes taking place in the eastern part of the Gulf Stream area, supplemented by uptakes from the eastern Gulf of Mexico. The uptakes in Meanwhile, the central North Atlantic contributed about contributes approximately 20% to the total moisture content prior to ascent. Overall, the primary contributions can therefore be attributed to the area of the strongest CAOs before ascent.

Conversely, for NPVA nonGS trajectories, moisture is mainly sourced from the regions characterized by weak or absent CAOs and notably diminished surface fluxes (Fig.5a,b). Predominant moisture contributions stem from the Gulf of Mexico's subtropical regions and the Caribbean Sea (Fig. ??a), aligned 5f). A distinct observation for the NPVA nonGS trajectories is that their moisture uptakes within the Gulf of Mexico are positioned further to the west, compared to those of NPVA GS trajectories (Fig.5e-f).

The primary uptake regions for NPVA GS trajectories not only align with the Gulf Stream SST front — Overall, CAOs play a crucial but also correspond to areas of intense CAOs (Fig.5a), which seem to play a significant role in the life cycle evolution of NPVA GS trajectories. On average, 56.2% of all moisture uptakes occur happen during CAO events over the ocean when the atmosphere is colder than the surface (dark blue line in Fig. ??a). Around 16% of these CAOs overlap with the uptake location in the cold sector of the cyclone (, when the cold, continental air is advected over warmer water surface (green line in Fig. ??a). Moreover, a substantial proportion of moisture uptakes transpire during more intense

CAOs (2K, light blue, dashed line in Fig.??a), accounting for over 31% of all uptakes. Only about 5% of the uptakes occur in the cold sector of the cyclone when it is not associated with a CAO (depicted by the brown line in Fig.6b). Some of the moisture uptakes, especially between 19 and 23 February, align with intense SLHF events (Fig.6a). On the other hand, the NPVA nonGS trajectories tell slightly a different story: only 43% experience a CAO during moisture uptake, and the surface evaporation events observed during the same time frame in February were weaker for these trajectories (Fig.6a). Figures ??a and b demonstrate that a high fraction of CAO uptakes coincide with upward SLHFs exceeding 100 W/m^2 .

Moreover, these high heat flux events predominantly occur either before or during the formation of rapidly intensifying cyclones, as shown in Figure ??a. For example, the proportion of CAOs and the intensity of SLHFs were remarkably high between February 12–15. These intense SLHF events are likely tied to pronounced CAOs, potentially triggered by cyclones L1 and 15, preceding the rapid intensification of Cyclone LE0. Another similar event was observed around February 21, just before the rapid growth of LE2. The most recent peak in the CAO fraction, accompanied by intense surface evaporation, took place before the intensification of cyclone LE3 around February 25–26 (Figures ??a and ??). The relatively small number of uptakes occurring in the cold sector of the cyclone (brown and green lines in Figure ??a) compared to the large fraction of uptakes in CAO regions implies that uptakes primarily occur in the CAO induced by the cyclone, rather than directly in the cold sector of the cyclone causing the CAO. It is worth noting that the episodes of extreme SLHF are significantly larger in magnitude for the NPVA GS trajectories than for the NPVA nonGS trajectories (Figure ??b).

Our results are in agreement with other studies (e.g. Papritz and Grams, 2018; Aemisegger and Papritz, 2018; Hawcroft et al., 2012), indicating that CAOs play an important role in the water cycle of cyclones L2 (Fig.3). High surface heat fluxes, as pointed out by Tilinina et al. (2018), indicate that the cyclones responsible for these pronounced fluxes usually have greater depth and undergo quicker intensification. Our results support this perspective, as the highest fluxes experienced by NPVA GS air parcels coincide with the period when cyclones L1 and L2 are present in the North Atlantic (Fig.6a). As depicted in Figure 2d and 2f, both cyclones triggered significant CAO events, which affected many of the NPVA GS air parcels present at the time in the lower troposphere. When focusing specifically on these trajectories, we observe that the average uptakes occurring in CAOs are consistently more intense than those outside CAOs, particularly between 19 to 22 February (Fig.6c). This observation is consistent with insights from other studies (e.g. Papritz and Grams, 2018; Aemisegger and Papritz, 2018; Hawcroft et al., 2012), which highlight the pivotal role of CAOs in moisture-related dynamics. However, it remains poorly understood how air parcels moistened in the region behind a passing cyclone's cold front end up in the upper-level NPVA. One possible explanation is the existence of the so-called 'hand-over' mechanism described in detail by Papritz et al. (2021). They found that moisture precipitating in deep North Atlantic cyclones originates in the cold sector of a preceding cyclone and is fed into the ascent regions of the subsequent cyclone via the feeder air stream (Dacre et al., 2015).

To better understand moisture transport mechanisms in our case study, and explore the possibility of the 'hand-over' mechanism, we analyzed the relationship between in our case study we now use the surface latent heat flux (SLHF) and atmospheric trajectories. from ERA5 as a proxy for surface evaporation and relate it to the NPVA trajectories. Following the methods of Yamamoto et al. (2021) and Tilinina et al. (2018), we identified regions of maximum SLHF experienced by beneath the trajectories to locate areas of most intense evaporation and heating the areas of the most intense

surface evaporation. We also examined the locations where the ~~trajectories ascend~~ trajectory ascent into the upper troposphere
575 begins (Fig.??7).

Figure ??7a (red contours) illustrates the analysis for 24 February at 21:00 UTC, revealing that when air parcels of NPVA GS trajectories experience the most intense evaporation ~~occurs underneath, they are located below 800 hPa~~ near the Gulf Stream and in areas with the highest CAO index values. ~~Trajectories~~ The air parcels do not ascend immediately but remain in the atmospheric boundary layer for at least 24 hours, being advected south and southeast with the cold air in the cyclone's cold
580 sector (green contours in Fig.??7a). The ascent occurs approximately 54 hours after the maximum SLHF values (blue contours in Fig.??7b), suggesting that the ascent ~~is not directly~~ might not be caused by the cyclone responsible for strong surface evaporation. Instead, our findings suggest that cyclone ~~LE2-L2~~ (Fig.??3a) and ~~secondary cyclones L1 and L2 (Fig.??b) play~~ subsequent cyclones might have a significant role in lifting the moistened air parcels into the upper troposphere's NPVA, ~~which is consistent with the results reported.~~ This hypothesis aligns with the insights presented by Papritz et al. (2021). Cyclone ~~LE2~~
585 ~~travels through and intensifies in the region of L2 traverses and strengthens within the region marked by a strong CAO left~~ behind by LE1 in the wake of L1 (Fig.??b). ~~The already moistened air is then fed~~ 2b and d). This moisture-rich air potentially gets channeled into the ascending airstream of the LE2 cyclone. ~~Additionally, cyclones flow of the L2 cyclone. Moreover,~~ secondary cyclones following L1 and L2 develop behind LE1 lifting some of the could elevate portions of these air masses into the upper ~~troposphere layers~~ (Fig.2c).

To ~~confirm that the process described above dominates in the present~~ explore whether the process detailed above is dominant
590 in our case study, we ~~performed the analysis shown in Figure ??~~ conducted the analysis depicted in Figure 7a for all the NPVA GS trajectories (Fig.??7c). Analyzed trajectories experience the most intense moistening along the Gulf Stream SST front (red contours). One day later, the moistened air moves south or southeast, together with the air in the cyclone's cold sector (green contours). Trajectories begin their ascent into the upper troposphere (blue contours) on average 3.5 days after reaching
595 maximum SLHF values (Tab.2). ~~The time~~ 3). This is very much in line with the exemplary trajectory discussed before and in stark contrast to NPVA nonGS trajectories. The latter primarily experience regions of strongest surface evaporation in the subtropics near 20°N, and remain there before making their ascent further north at a later time (Fig.7d). The lingering of NPVA GS trajectories at low levels suggests that the involvement of multiple cyclones might be necessary to create conditions conducive to the moistening of trajectories followed by their ascent.

This notion is further supported by the analysis of the time difference between the ~~maximum SLHF~~ time trajectories
600 experienced the strongest moisture uptake and the time ~~of~~ when they start to ascend and their pressure drops below 800 hPa (Fig.8). For NPVA GS trajectories, longer delays between strongest moisture uptake and time of ascent are typical (green shading, Fig.8). The probability density function shows a plateau between peaks at 20 hours and 60 hours, Although the density drops thereafter a plateau extending from 70 to 150 hours. The 20-hour peak corresponds to trajectories ascending directly from
605 the Gulf Stream region (blue contours, Fig.7c). The second peak, coupled with the high density of values exceeding 100 hours, implies a significant temporal gap between moisture uptake and the start of ascent for the majority of NPVA GS trajectories. In contrast, NPVA nonGS trajectories show a single peak around 40 h and thus a rather immediate ascent after experiencing the strongest moisture uptake.

The statistics and results presented thus far hint at the potential presence of a ‘hand-over’ mechanism in our case study. However, to truly identify its presence and understand how signals from the Gulf Stream air-sea interactions are related to the upper troposphere, we delve deeper by computing various metrics for each trajectory’s initiation time. These metrics include average trajectory positions, density of strongest moisture uptakes, and the average times of ascent and strongest moisture uptake. Next, we plot these metrics alongside cyclone masks during the times of moisture uptake (represented by green contours) and the start of ascent (represented by red contours). Visual representations of this analysis are provided in figures 9 and 10 and in the Supplementary Materials (for each time step of the case study).

Exemplary we show NPVA GS trajectories initialized on 21 February 2019 at 12:00 UTC and for illustrative purposes distinguish those which initially cross the Gulf stream on a southeastward track (towards the region south of 30° N and east of 50° W) from those which approach the Gulf Stream from the South. The former subset amounts to about 25% of the NPVA GS dataset for trajectories started on 21 February 2019 at 12:00 UTC. Ten days before their start, these trajectories are positioned over the Gulf Stream region, where they first begin to accumulate moisture (Fig.9a). They subsequently descend further to the central North Atlantic, where they gather the majority of their moisture over a span of several days (purple shading in Fig.9a). On average, this moisture accumulation occurs 192 hours prior to their initialization (green dot, Fig.9a). Following this, their ascent is consistent with a hand-over from one cyclone to another. In line with the findings of Papritz et al. (2021), air parcels collect moisture in the region of intense surface evaporation behind the cold front of a cyclone. Their ascent into the upper troposphere is possible thanks to the passage of a second cyclone, that travels into the region starts roughly 123 hours after the moisture uptake (red dot, Fig.9a). It is important to note the presence of cyclones south of Greenland during both the moisture uptake (green contours) and ascent stages (red contours), with each phase associated with distinct cyclones. A substantial number of the moisture uptakes happen in the CAO region (Fig.9b), in the wake of cyclone I0, whereas the ascent primarily occurs in the warm sector of cyclone II (Fig.9c).

Also for the remaining majority of high surface fluxes. This notion is further supported by the observation that more than 76% of the NPVA GS trajectories start their ascent more than a day after passing through the region of the most intense SLHF. Furthermore, they remain in the ABL for (75%) started on 21 February 2019 at 12:00 UTC, the Gulf Stream region emerges as the primary moisture source. On average, these trajectories accumulate moisture about 156 hours before their initialization (green dot in Fig.10a). At that time (-156 h) cyclone L0 (green contour) is located south of Greenland, with a CAO event developed in its wake and in the Gulf Stream region (Fig.10b). The ascent of those trajectories takes place ~4 days prior to 102 hours later ahead of cyclone L1 (red dot and contours, Fig.10a,c).

While a sequence of cyclones is pivotal for the moistening and ascent of most trajectories in our study, it is the specific trajectories that traverse the central North Atlantic that very clearly exhibit the ‘hand-over’ mechanism described by Papritz et al. (2021) (Fig.??). These represent about 30% of all NPVA GS trajectories, peaking at 65% for some starting times. They most closely align with the ‘hand-over’ mechanism, as they seem to be fed into the cyclone moving into the central North Atlantic. For the other trajectories (Fig.10), there is less evidence for a ‘hand-over’ mechanism, thus it is challenging to discern whether this mechanism or the sequential appearance of cyclones is more pivotal for their development. Nevertheless, one consistent observation stands out when looking at figures 10a, 9a, and the Supplementary Material: the presence of a cyclone south of

	NPVA GS trajectories	NPVA nonGS trajectories
Average time of moisture uptake prior to the start of ascent.	3.5 days <u>3.5 days (-84 h)</u>	3.8 days <u>(-92 h)</u>
Fraction of moisture supplied within first 5 days <u>backward</u> .	60%	48%
Fraction of moisture uptakes over the ocean.	78%	44%
Average time of ascent start in <u>relative relation to</u> the time of arrival into the NPVA.	-2.6 days <u>(-63 h)</u>	-6.65 days <u>(-159 h)</u>
Average time in the ABL prior to ascent.	4 days <u>(96 h)</u>	3.8 days <u>(91.2 h)</u>
Average time of continuous SLHF<0 W/m ² prior to the start of ascent.	2.5 days <u>(60 h)</u>	23 h

Table 3. Summary of general characteristics and moisture sources for NPVA GS and NPVA nonGS trajectories.

645 Greenland. Intriguingly, while both moisture uptake and ascent events feature a cyclone in this position, distinct cyclones are responsible for each of these processes. This suggests that a series of cyclones plays a pivotal role — initially moistening the NPVA GS trajectories thanks to the ascent and are continuously subjected to surface evaporation for ~2.5 days (Tab. 2). Such a long exposition to negative SLHF supports the notion that they are advected with passage of one cyclone, and subsequently lifting them into the upper troposphere with a subsequent cyclone. Moisture uptake can occur directly in the wake of a cyclone, during a CAO event initiated by the cold air behind the cyclone’s cold front. Given those statistics, as well
650 as the dominance of the CAO trajectories in the NPVA GS dataset (Section ??), we propose that during the passage, or in the cold sector of secondary cyclones that develop following a strong primary cyclone. This observation is consistent with findings from Papritz et al. (2021) and Dacre et al. (2019). They highlighted the localized origins of moisture sources for North Atlantic cyclones and underscored the significance of consecutive cyclone appearances in shaping the region’s moisture cycle.

655 Based on the above findings, we conclude that during our study period, the ‘hand-over’ process is the dominating pathway for moisture transfer in the North Atlantic for air masses that interact directly with the Gulf Stream—a succession of cyclones was essential for the evolution of trajectories crossing the Gulf Stream (NPVA GS trajectories). This pathway enabled them to accumulate moisture and subsequently rise into the upper troposphere, thereby influencing the block’s dynamics. Our analysis thus sheds light on the mechanisms through which signals from Gulf Stream air-sea interactions reach the upper layers of the atmosphere. This understanding might also clarify why changes in SSTs in the western North Atlantic in model simulations
660 lead to alterations in large-scale dynamics (e.g. Czaja et al., 2019; Athanasiadis et al., 2022; Scaife et al., 2011).

3.4 ~~Moisture sources for NPVA nonGS trajectories~~

~~For backward trajectories that did not interact with the boundary layer-~~

4 Synthesis and Discussion

Our detailed case study of a European Blocking event in February 2019, offers insights into how air-sea interactions over the Gulf Stream, the primary moisture sources are located in the Gulf of Mexico and the Caribbean Sea (Fig.??d), with smaller contributions found in the North Atlantic and the eastern Pacific Ocean.

Similar to NPVA GS trajectories, NPVA nonGS trajectories acquire moisture around 3.8 days prior to ascent (shown as blue dashed bars in Fig.??a and Tab/2). The majority (67%) of this moisture is acquired within the first seven days of ascent, with 48% being acquired within the first five days (blue line in Figure 5a). NPVA nonGS trajectories tend to have a higher number of uptakes compared to NPVA GS trajectories, accounting for 75% may be associated with the dynamics of an upper-level ridge. Although air masses identified as interacting with the Gulf Stream represent roughly 12% of all trajectories originating within the block's region, we show evidence of their disproportional role in maintaining or enhancing the block's persistence. The potential importance of those air masses for the development of the block can be established based on the results of Steinfeld et al. (2020), who determined that critical features of the block, including extent, strength, and lifetime, are strongly affected by latent heating taking place in the ascending air streams. Our analysis revealed that almost all of the Gulf Stream trajectories (representing ~12% of all NPVA base trajectories and ~28% of all ascending ones, Tab.1.2) experience diabatic heating during the first three days after starting from the blocking region. Additionally, trajectories -However, only 44% of these uptakes occur over the ocean, which is significantly lower than the 75% of trajectories that interact with the Gulf Stream (Tab.2. NPVA nonGS trajectories take an average of 6.65 days to ascend into the upper-level NPVA from the time they leave the atmospheric boundary layer (shown as blue dashed bars in Fig.??b). This suggests that the area of ascent for these trajectories differs from that of the NPVA nonGS trajectories (as shown exhibit a significantly higher proportion of diabatically heated trajectories (98%) than those not traversing the Gulf Stream (54.7%).

Our findings reveal that air often warmed and moistened in the CAO regions induced by one cyclone, ascends into the upper troposphere through the upward air stream of a subsequent cyclone. This observation aligns with studies by Papritz et al. (2021); Dacre et al and Sodemann and Stohl (2013), and the process is graphically illustrated in Fig. ??e).

The CAO index 11. When cyclone L0 traverses the western North Atlantic, it induces a CAO just behind its cold front (Fig.??a) shows that weak CAOs in February 2019 took place also over the eastern Pacific Ocean. In consequence, on average 45% of NPVA nonGS trajectories experienced a CAO. Around 13% of those moisture sources were located over the ocean, in the cold sector of the cyclone. Surface evaporation events were not as intense or as frequent for the NPVA nonGS trajectories as they were for the NPVA GS trajectories (blue colors in Fig.??b). This is also confirmed by the spatial distribution of CAOs (Fig. ??a), SLHF (Fig.??b), and moisture sources 11a). This event sets the stage for atmospheric boundary layer warming and moistening. The most robust heat fluxes are observed along the Gulf Stream SST front, a consequence of the pronounced air-sea temperature gradient. It is also where the majority of trajectories undergo moisture uptake. Intriguingly, a subset, constituting about 15% in the presented case and referred to as 'recirculating trajectories' (Fig.??d). The regions supplying moisture for the NPVA nonGS trajectories are identified as areas of weak or nonexistent CAOs and substantially weaker surface fluxes 11a), travels further into the central North Atlantic. As they traverse, these trajectories are exposed to additional moisture from the milder CAOs that form in the aftermath of cyclone L0, as well as from secondary cyclones that emerge in its trail (Fig. ??a,b). The highest moisture contributions are found in the subtropical regions of the Gulf of Mexico and the Caribbean Sea

(Fig. ??f). It is noteworthy that, in contrast to the uptakes for NPVA-GS trajectories, the uptakes in the Gulf of Mexico are located further west (Fig. 3a). 51 hours later, a new cyclone, labeled L1, emerges at the same spot previously occupied by cyclone L0. This new cyclone has traveled through and gained strength in the regions marked by CAOs - zones of heightened air-sea interactions - originally induced by cyclone L0. Consequently, the pre-moistened and warmed air is channeled into the warm sector of cyclone L1, which provides conditions for its ascent into the upper layers of the troposphere. Overall, in our results, the 'hand-over' mechanism is especially pronounced for trajectories labeled as 'recirculating' ones (Fig. ??e-f). Moistened air masses of NPVA nonGS trajectories remain in the atmospheric boundary layer for ~3.8 days prior to ascent, but maintain negative SLHF for only ~23 h (Tab. 2)

The NPVA nonGS trajectories have two primary regions of ascent (Fig. ??, d). Air masses that experience intense moistening in the subtropical Caribbean Seas start their ascent (Fig. 11). Their behavior closely mirrors the feeder air stream concept described by Papritz et al. (2021) and Dacre et al. (2019). While a significant portion of the trajectories show limited evidence for the existence of a 'hand-over' mechanism, our analysis emphasizes a key insight: a minimum of two cyclones is essential for trajectories, which interact with the Gulf Stream, to undergo both moistening and subsequent ascent into the upper troposphere over the southern coast of the United States (Fig. ??, d). Whereas the trajectories with the highest SLHF over the eastern Pacific begin their upward movement in the same area where they pick up moisture. Additionally, our data highlights a potential preconditioning by a preceding cyclone, creating favorable conditions for the succeeding cyclone. This is evident as cyclones in our study frequently traverse and amplify within CAOs, caused by preceding cyclones (Fig. ??d; Fig. ??d). In comparison to the NPVA-GS trajectories, which ascend straight into the upper-level NPVA, (2).

The Gulf Stream region serves as an important moisture source for those NPVA trajectories that passed over it in the lower troposphere, in agreement with the results of Yamamoto et al. (2021) and Pfahl et al. (2014). In fact, the Gulf Stream contributes most of the locations of the ascent of NPVA nonGS trajectories are further away from the blocking region. This explains why the time needed for the NPVA nonGS trajectories to reach upper-level NPVA, from the time they leave the atmospheric boundary layer, is much longer (~6.65 days). Upon ascending into the upper troposphere, those air masses are then advected into the block and do not interact directly with the extratropical cyclones developing moisture present in the air prior to its ascent. Those findings imply that the moisture sources for extratropical cyclones in the North Atlantic or CAOs in the Gulf Stream region.

725 4.1 Properties of GS NPVA trajectories

The results shown above indicate that the water cycle of extratropical cyclones in the North Atlantic is substantially influenced by the have a regional character and are concentrated in areas where there is a strong ocean-atmosphere temperature contrast. Another area of moistening of the atmospheric boundary layer is found in the central North Atlantic, south of the Gulf Stream's eastward extension. This area is frequently affected by the advection of cold air from the Labrador Sea or the passage of a cyclone, which provides conditions for strong air-sea interactions over the Gulf Stream. The significance of interactions. In fact, the processes taking place over the warm waters of the Gulf Stream can be established even more clearly by taking a closer look at the temporal variations in the GS NPVA trajectories' properties. In this section, we will focus on the GS

NPVA trajectories, since their higher spatial resolution (50 km) is more suitable for an in-depth analysis of the properties of air that have passed over the Gulf Stream and contributed to the formation of the block over western Europe. cyclones recognized as rapidly intensifying propagate into this stretch of the ocean, while several of the secondary cyclones originate there (Fig.3). The consistent occurrence of cyclones in areas with intense surface evaporation suggests a 'preconditioning' for cyclone development, as described by (Papritz et al., 2021).

Analysis of pressure changes along the trajectories shows that ascent towards the block takes place within 2-3 days after leaving the Gulf Stream region (Fig. ??a). Air masses that interact with the warm waters of the Gulf Stream typically originate from the mid and lower troposphere, and upon passing through the It should be noted that the subtropical regions of the Caribbean Seas and eastern North Pacific are significant moisture sources for air streams progressing to the block, with the NPVA nonGS trajectories comprising 72% of the trajectories. However, these air streams predominantly ascend in regions such as the Gulf of Mexico and the Pacific Ocean, which lie outside the main cyclonic activity in the western North Atlantic; travel into the NPVAs in the upper atmosphere. The potential temperature changes during the ascent highlight the importance of diabatic processes, which, as previously mentioned, occur in all of the GS NPVA trajectories (Fig. ??b, Fig. ??b).

Furthermore, the high sensible and latent heat fluxes experienced by. Therefore, for the air masses that ascended into the block during the extratropical cyclones of February 2019 in the trajectories as they interact with the atmospheric boundary layer over the Gulf Stream can be attributed to the influence of CAOs (Fig. ??c-d). The North Atlantic, these distant moisture sources seem less influential.

A study by Papritz and Grams (2018) suggests that weather regimes modulate the occurrence of CAOs. However, our findings present a more intricate picture where this relationship appears mutual. During our observed period, CAOs predominantly arose due to the advection of cold air across the warm waters of in the wake of cold fronts from passing cyclones, particularly in the Gulf Stream leads to significant heat and moisture exchange between the ocean and the atmosphere, resulting in an increase of specific humidity (Fig. ??f). The period of strong moistening and heating of GS NPVA trajectories in the lower troposphere coincides with a significant decrease of potential vorticity (Fig. ??e). In fact, we determined, that a large number of trajectories have negative PV in the lower troposphere region and its extension. Such CAOs not only induce intense surface heat fluxes, which are essential for maintaining baroclinicity (Papritz and Spengler, 2015), but also play pivotal roles in sustaining the storm track (Aemisegger and Papritz, 2018). Furthermore, they promote the formation of rapidly intensifying low-pressure systems, essential for the growth of atmospheric blocks (Colucci, 1985; Colucci and Alberta, 1996). In tandem, these CAOs create conditions favorable for vigorous evaporation events in the western North Atlantic. This abundant moisture aids the swift intensification of cyclones and the genesis of secondary low-pressure systems, contributing to the northward expansion of an upper-level ridge. This, in turn, weakens the zonal flow, paving the way for further CAO development and subsequent intense surface evaporation events (Kautz et al., 2022; Gao et al., 2015). It is important to highlight that negative PV anomalies only occur for a limited number of time steps and at different time steps for each of the considered trajectories also worth noting that these pronounced oceanic evaporation events are instrumental for the emergence of WCBs (Pfahl et al., 2014; Eckhardt et al., 2004) , responsible for the emergence of low PV anomalies in the upper troposphere (Pfahl et al., 2015; Steinfeld and Pfahl, 2019; Methven, 2015

770 While our study concentrates on a limited set of trajectories in comparison to all initiated from the NPVA objects, such a subset, as suggested earlier, might have implications in the reinforcement or sustenance of the block. Consequently, when visualizing the median, 10th, and 90th percentiles in plots (such as Fig. 3) we hypothesize that the block's termination could be linked to a reduced ocean heat content following the passage of several cyclones. This reduction could diminish air-sea interactions, atmospheric heating, and moistening, which in turn impacts the storm track (as evidenced by the altered pathways of cyclones L3 and L4, Fig. 3) and the intensity of the cyclones. ~~??~~—these negative PV anomalies may not be evident.

Nevertheless, the presence of negative PV suggests that very intense mixing or cloud-related evaporative processes are

775 5 Conclusions

To summarize, our study provides a possible explanation for a mechanistic link between air-sea interactions over the Gulf Stream region and the formation of blocks over the North Atlantic and European regions. It also underscores the potential significance of CAOs and the associated strong air-sea interactions in the formation or preservation of a quasi-stationary, upper-level ridge. In light of the growing evidence suggesting that biases in North Atlantic SST representation are linked to model inaccuracies in block prediction (e.g. Athanasiadis et al., 2022; Czaja et al., 2019; Kwon et al., 2020), it is vital to clarify how the processes taking place in the cold sector of cyclone (Attinger et al., 2019; Crezee et al., 2017; Attinger et al., 2021) —Furthermore, low-potential vorticity air in the inflow region of lower troposphere over the western North Atlantic are connected with the dynamics in the upper levels. Additionally, the WCB can significantly impact the development of NPVAs in the upper troposphere (Methven, 2015; Teubler and Riemer, 2016) recurrent influence of SST observed in climatological studies (Michel et al., 2023; Omrani et al., 2019; Scaife et al., 2011) implies that the mechanisms linking the Gulf Stream, diabatic processes, and large-scale extratropical circulation might hold relevance on a climatological scale. Nevertheless, it is essential to note that a single case study cannot be used to draw any general conclusions. However, considering the fact that singular aspects of our analysis are in agreement with recent publications focusing on moisture transport in the North Atlantic and the formation of blocks (e.g. Papritz et al., 2021; Aemisegger and Papritz, 2018; Hirata et al., 2019; Yamamoto et al., 2021; Steinfeld et al., 2020; Dacre et al., 2021), it provides a basis for further research. Therefore, a closer examination of the changes in PV along GS-NPVA trajectories is carried out in a subsequent study, we are going to analyze those relationships using a similar trajectory dataset spanning 40 years of ERA5 data. Using the methods applied in this case study, we will aim to establish whether the air-sea interactions over the Gulf Stream modulate the large-scale dynamics and formation of blocked weather regimes over Europe and to identify the predominant way by which the signal from the lower troposphere is transferred to the upper-level flow.

795 5.0.1 Negative Potential Vorticity in the lower troposphere

Appendix A: Negative Potential Vorticity in the lower troposphere

~~Overall, approximately 76%~~ In the course of our study, we consistently observed the presence of negative PV during the inflow stage of trajectories, defined as the phase preceding ascent when trajectories are confined within the atmospheric boundary

layer (pressure exceeding 800 hPa). Upon further examination, we found that 82% of ~~the GS-NPVA trajectories have negative~~
800 ~~PV in the lower troposphere over the ocean at some time prior to ascent~~. In agreement with these results, when the same
~~analysis is applied to the NPVA GS trajectories –82% have negative PV in the atmospheric boundary layer~~displayed negative
PV values at certain intervals prior to their ascent. Given the potential significance of this feature (Methven, 2015), we chose
to examine it more closely.

To explore the role of air parcels with negative PV in the formation of upper-level negative PV anomalies (NPVAs) we
805 divided the ~~GS-NPVA-NPVA GS~~ trajectories into two subsets: those with negative PV (~~GS-NPVA-NPVA GS~~ negPV trajectories,
~~76~~82% of all ~~GS-NPVA-NPVA GS~~ trajectories) and those with continuous positive PV (~~GS-NPVA-NPVA GS~~ posPV trajectories,
~~24%~~18% of ~~GS-NPVA-NPVA GS~~ trajectories) in the lower troposphere. To investigate the potential influence of negative
PV in the lower troposphere on the formation of upper-level NPVA, we examined the inflow and outflow stages of ascent.
Specifically, we re-centered the time evolution of the trajectories ~~on the level at the time~~ of maximum heating, which is
810 indicative of the release of latent heat during upward air mass movement. By comparing the two sets of trajectories, we aim
to determine whether the presence of negative PV air in the inflow stage of the ascending air stream leads to the formation of
low PV air in the upper troposphere. Our results show that the ~~GS-NPVA-NPVA GS~~ negPV trajectories are located in the lower
layers of the troposphere (Fig. ~~??A1~~a) and experience more intensive heating during the ascent (Fig. ~~??A1~~b). Without indicating
a cause-and-effect connection, greater fluxes in the inflow stage (Fig. ~~??A1~~c-d) and elevated moisture content during the ascent
815 (Fig. ~~??A1~~f) co-occur with a rise in heating intensity throughout the ascent. Interestingly, despite experiencing negative values
of PV in the atmospheric boundary layer and a strong heating rate, the PV of the ~~GS-NPVA-NPVA GS~~ negPV trajectories is
not lower than that of the ~~GS-NPVA-NPVA GS~~ posPV trajectories in the upper troposphere (Fig. ~~??A1~~e) nor do they reach a
higher outflow height (Fig. ~~??A1~~a,b). In fact, the ~~GS-NPVA-NPVA GS~~ negPV trajectories typically begin at a lower altitude,
and as a result, more heating is required for these trajectories to achieve a comparable outflow height to that of the ~~GC-NPVA~~
820 ~~NPVA GS~~ negPV trajectories. Surprisingly, the PV values in the ~~GS-NPVA-NPVA GS~~ negPV trajectories are even slightly
higher when reaching the upper troposphere. ~~Additionally, we observe that the air masses maintaining~~ Furthermore, we note
that air masses with only positive PV values ~~interact with the CAOs to a lesser degree, as~~ have limited interactions with CAOs.
This is evident from the temporal ~~changes of sensible heat flux variations of latent and sensible heat fluxes observed~~
~~types of trajectories. Indicating that processes occurring during CAOs may be responsible for the decrease of trajectory types.~~
825 In fact, our analysis reveals that 85% of negative PV values are located within CAO regions. This suggests that the processes
during CAOs might play a pivotal role in reducing PV in the atmospheric boundary layer.

There are several processes that can result in the destruction of PV in the lower troposphere, including friction, evaporative
cooling, sublimation of snow, snow melting, or turbulent fluxes (Crezee et al., 2017; Attinger et al., 2019, 2021). To establish
what mechanism leads to ~~the~~ PV destruction throughout our case study, we examined vertical ~~cross-sections~~ cross-sections
830 of cloud liquid water content and potential vorticity over the area of the Gulf Stream. For the purpose of this analysis, we
used the ERA5 reanalysis dataset with a higher temporal resolution of 1 hour. Obtained results reveal that the air parcels with
negative PV in the lower troposphere are primarily located below liquid water clouds (Fig. ~~??b~~A2a), in the cold sectors of
the cyclones (Fig. ~~??3~~, Fig. ~~??a~~A2c). The cold sector ~~can be recognized in Figure ??b at approximately 36~~ is evident in Figure

835 ~~A2a around 40°N latitude by looking at, identifiable by~~ the cloud structure. ~~It can also be discerned in Figure A2b based on~~
~~the temperature contrast. It should be highlighted that these cross sections represent values averaged between -50° and -60°~~
~~W. Thus, to accurately assess the locations of air parcels, one should refer to Figures a, b, and c collectively.~~ Clouds in the
warm sector of the cyclone extend deep into the atmospheric boundary layer, while the cold sector is dominated by low-level
stratiform clouds. Low-level clouds forming during the advection of cold air over the ocean due to the cooling of the surface
are classified as stratiform clouds (Painemal et al., 2021). The presence of air parcels with negative PV in those areas suggests
840 that evaporative cooling is the main cause of PV reduction. This was confirmed by Chagnon et al. (2013), who discovered that
evaporative cooling in the air descending behind the cold front decreases PV. This idea is further reinforced by the studies of
e.g., Wood (2005), Jensen et al. (2000) and Paluch and Lenschow (1991), who found that evaporative cooling in the sub-cloud
layer of stratiform clouds is often triggered by the cooling that results from drizzle evaporation.

In most of the analyzed timesteps (e.g. Fig. ~~??A1~~) the PV in the lower troposphere does not ~~exceed go below~~ -1 PVU.
845 However, for several air parcels, we found values below -2 PVU in the two lowest model layers right behind the cold front.
Attinger et al. (2019) and Vanni re et al. (2017a) attribute the prevalence of negative PV along the cold front to unstable
conditions and high surface fluxes. This ~~likely also applies applies also~~ to our case, as the high negative PV values are found
at low altitudes, in the regions of very intense surface fluxes, mainly during the intensification stage of the extreme cyclones
(Fig. ~~??3a~~). Overall, we presume that the combination of strong surface fluxes, heating from the surface, and evaporative cooling
850 from low clouds leads to the development of a highly unstable environment, making the presence of negative PV in our case
so widespread.

It is worth highlighting that a significant number of air parcels in Figure ~~??a A2~~ have negative PV and are positioned ahead
of the cold front. Our analysis of consecutive time steps reveals that these parcels are transported to this location due to the
advection of cold air that trails the cold front from a preceding cyclone. ~~Considering the handover mechanism's predominance~~
855 ~~in our case study and the findings presented in Figure ??, it is reasonable to expect that their PV will increase within the next~~
~~few hours and they will be carried upwards into the upper troposphere by the ascending airstream of cyclone LE1 (Fig. ??).~~

Appendix B: ~~Synthesis and Discussion~~

~~Our study suggests that air-sea interactions over the Gulf Stream are closely linked to the development of the European~~
~~Blocking event in February 2019. Furthermore, our findings raise the possibility that a similar relationship may exist at a~~
860 ~~climatological level, indicating that air-sea interactions over the Gulf Stream could be relevant for other blocking events in the~~
~~North Atlantic-European region. Trajectory analysis reveals that on average 60% of all GS trajectories started from the Gulf~~
~~Stream end up in the blocking region, representing approximately 23% of all trajectories that formed the NPVAs. The potential~~
~~importance of those air masses for the development of the block can be established based on the results of Steinfeld et al. (2020)~~
~~, who determined that critical features of the block, including extent, strength, and lifetime, are strongly affected by latent~~
865 ~~heating taking place in the ascending airstreams. Our analysis revealed that all of the Gulf Stream trajectories (representing~~
~~~23% of all trajectories) experience diabatic heating during the first three days after starting from the blocking region. Given~~

that approximately 49% of trajectories released from the NPVAs undergo diabatic heating, our results suggest that air masses interacting with the Gulf Stream may play a considerable role in the blocking formation (see Section ??).

870 Our analysis shows that air moistened and warmed in the CAOs generated by the passage of a cyclone is lifted into the upper troposphere with the ascending air stream of a consecutive cyclone, in agreement with Papritz et al. (2021) and Sodemann and Stohl (2013). This mechanism is schematically depicted in Fig. ?? The passage of a cyclone marked as LE1 (Fig. ??a) over the western North Atlantic results in the development of a CAO behind the cold front (Fig. ??a), providing conditions Given the sequence of cyclones previously described as necessary for the moistening and heating of the atmospheric boundary layer. The strongest fluxes are found along the Gulf Stream SST front, as the air-sea temperature contrast is the largest  
875 in this region. 30 hours later, cyclone LE1 is located near the southern tip of Greenland, while two smaller cyclones ascend of trajectories, it is plausible to assume that these air parcels, having interacted with a CAO induced by one cyclone, will subsequently ascend into the upper troposphere with cyclone L1 and L2 developed in the central North Atlantic (Fig. ??b). The ascending air streams of those cyclones lift some of the air masses, that were moistened and heated in the cold sector of cyclone LE1, into the upper troposphere. Moreover, the air-sea interactions in the cold sectors of cyclones L1 and L2 result  
880 in further heating and moistening of the atmospheric boundary layer in the central North Atlantic. At the same time, a third cyclone develops, LE2, which travels into the region of large surface latent and sensible heat fluxes created by cyclones L1, L2, and LE1. The air, moistened thanks to the advection of cold air by these cyclones is fed into the warm sector of cyclone LE2 and begins its cross-isentropic ascent into the upper troposphere. Therefore, in agreement with Papritz et al. (2021) and Daere et al. (2019), this suggests that one cyclone provides the environment favorable for the intensification of a consecutive  
885 cyclone. The air masses, heated and moistened in the cold sector of the first cyclone, are later fed into the warm sector of the consecutive cyclone and eventually lifted into the upper-level NPVA. (Fig.3)

The Gulf Stream region serves as an important moisture source for those NPVA trajectories that passed over it in the lower troposphere, in agreement with the results of Yamamoto et al. (2021) and Pfahl et al. (2014). In fact, the Gulf Stream contributes most of the moisture present in the air prior to its ascent. Those findings imply that the moisture sources for  
890 extratropical cyclones in the North Atlantic have a regional character and are concentrated in areas where there is a strong ocean-atmosphere temperature contrast. Another area of moistening of the atmospheric boundary layer is found in the central North Atlantic, south of the Gulf Stream's eastward extension. This area is frequently affected by the advection of cold air from the Labrador Sea or the passage of a cyclone, which provides conditions for strong air-sea interactions. In fact, the cyclones recognized as rapidly intensifying propagate into this stretch of the ocean, while several of the secondary cyclones  
895 originate there. The frequent presence of cyclones in a region of strong surface evaporation highlights the importance of 'preconditioning' for cyclone development described by (Papritz et al., 2021).

It should be noted that the subtropical region of the Caribbean Seas and eastern North Pacific serves as a significant source of moisture for air streams ascending to the block. However, it is worth emphasizing that the regions in which these air masses ascend, namely the Gulf of Mexico and the Pacific Ocean, are situated outside the western North Atlantic. Consequently,  
900 remote sources of moisture do not appear to be relevant for the air masses ascending into the block within the extratropical cyclones that formed in the North Atlantic in February 2019.

The occurrence of CAOs during the studied period is primarily due to the advection of cold air behind cold fronts of passing cyclones that develop in the Gulf Stream region and its extension. These CAOs not only lead to intense surface heat fluxes, which are essential for maintaining baroclinicity (Papritz and Spengler, 2015), but also contribute to the self-maintenance of the storm track (Aemisegger and Papritz, 2018) and the formation of rapidly intensifying low-pressure systems crucial for blocking growth (Colucci, 1985; Colucci and Alberta, 1996). Exceptionally strong oceanic evaporation events are vital for the development of WCBs (Pfahl et al., 2014; Eckhardt et al., 2004), which facilitate the transport of low-PV air into the upper troposphere (Pfahl et al., 2015; Steinfeld and Pfahl, 2019; Methven, 2015).

According to a study by Papritz and Grams (2018), weather regimes modulate the occurrence of CAOs, but our research indicates that this relationship may be mutual. CAOs that develop shortly before and during blocking create favorable conditions for strong evaporation events in the western North Atlantic, providing the necessary moisture for the rapid intensification of cyclones and the development of secondary low-pressure systems. These cyclones contribute to the northward expansion of an upper-level ridge, weakening the zonal flow and fostering further CAOs development, which in turn trigger intense surface evaporation events (Kautz et al., 2022; Gao et al., 2015).

The advection of cold air over warmer sea surfaces leads to air-sea interactions, which can result in the destruction of PV in the lower troposphere. Our research aligns with the findings of previous studies conducted by Crezee et al. (2017), Chagnon et al. (2013), and Attinger et al. (2019), which suggest that the presence of negative PV in the atmospheric boundary layer can be attributed to evaporative cooling beneath low-level stratiform clouds and strong surface fluxes.

In To summarize, in contrast to the hypothesis of Methven (2015), which proposes that the average PV of WCB outflow is nearly equal to the PV of its inflow due to an almost negligible net change in models, our study offers a slightly different viewpoint. In the analyzed case study, trajectories with negative PV in the atmospheric boundary layer (ABL) exhibit a somewhat higher PV in the upper troposphere when compared to trajectories with positive PV in the ABL. These findings imply that diabatic PV production and destruction may often not exactly balance during ascent as suggested by ?. This highlights the potential need for further research on the relationship between diabatic processes and changes in ascending air streams.

Our study demonstrates that NPVA objects forming the block are partially created and maintained by ascending air streams of subsequent cyclones developing in the North Atlantic, as indicated by low values of PV in the upper troposphere (Figs.?? and ??). However, Therefore, we cannot directly link the growth of NPVAs to the presence of negative PV in the atmospheric boundary layer. In our case study, negative PV functions more as a marker for an unstable environment and evaporative cooling associated with low-level stratiform clouds.

## 930 Appendix B: Conclusions

These findings imply that diabatic PV production and destruction may often not exactly balance during ascent as suggested by Methven (2015). This highlights the potential need for further research on the relationship between diabatic processes and changes in PV in ascending air streams.

To summarize, our study provides a possible explanation for a mechanistic link between air-sea interactions over the Gulf Stream region and the formation of blocks over the North Atlantic and European regions. It highlights the importance of CAOs and associated moisture uptakes and subsequent ascending air streams for the formation of a quasi-stationary, upper-level ridge. It is clear that a single case study cannot be used to draw any general conclusions. However, considering the fact that singular aspects of our analysis are in agreement with recent publications focusing on moisture transport in the North Atlantic and the formation of blocks (e.g. Papritz et al., 2021; Aemisegger and Papritz, 2018; Hirata et al., 2019; Yamamoto et al., 2021; Steinfeld et al., 2020), it provides a basis for further research. Additionally, an increasing number of recent studies indicate that biases in the SST representation in the North Atlantic are related to models' inability to correctly predict blocks (e.g. Athanasiadis et al., 2022; Czaja et al., 2020), thus suggesting that the mechanistic linkage between the Gulf Stream, diabatic processes, and the large-scale extratropical circulation found in our results are relevant on a climatological scale. Therefore, in a subsequent study, we are going to analyze those relationships using a similar trajectory dataset spanning 40 years of ERA5 data. Using the methods applied in this case study, we will aim to establish whether the air-sea interactions over the Gulf Stream modulate the large-scale dynamics and formation of all seven weather regimes (Grams et al., 2017) and to identify the predominant way by which the signal from the lower troposphere is transferred to the upper-level flow.

Synoptic evolution of European Blocking episode from February 2019. First column: potential vorticity (shading, PVU) at 315 K and negative potential vorticity anomaly objects (dashed contour) on 2019-02-18, 12:00 UTC (a), 2019-02-21 12:00 UTC (c), 2019-02-23 18:00 UTC (e), 2019-02-27 21:00 UTC (g). The major NPVA is shaded in grey and the minor in light blue (Section 2.1.3). Black crosses: locations of NPVA-GS trajectories on the specified dates on the 315 K ( $\pm 2$ K) isentropic level. Second column: 2 m temperature anomalies (with respect to a 30d running mean, shading) and upper level 2-PVU contour at 315K (green line), with PV values higher than 2 PVU shaded in green, for 12:00 UTC of each day from figures (a, c, e, g). LE0-3 and L1-2 refer to cyclones from Fig.??.

Tracks of cyclones formed in the North Atlantic between 15th and 27th Feb. 2019 together with contours of mean sea surface temperature throughout that period. (a) Rapidly intensifying cyclones (Sanders and Gyakum, 1980), the dates near the name of the cyclones e.g. 21,20:00, LE2 refer to the date and hours when the cyclones started to intensify rapidly; E in the name of the cyclone stands for extreme, (b) other cyclones, in color those relevant for the paper, in black other, non-rapidly intensifying cyclones. The dates in the legend for both (a) and (b) indicate the start of the cyclone track.

Cold air outbreak index (blue shading) and mean sea level pressure (black contours) in the North Atlantic and eastern Pacific on the dates when cyclones LE1, LE2, LE3 (Fig.??) start to intensify rapidly: (a) 2019-02-18, 18:00, (b) 2019-02-21, 20:00, (c) 2019-02-26, 03:00. LE1, LE2, LE3, L1, L2, L4 indicate positions of cyclones from Fig.?? on the chosen date.

The percentage of different subsets of trajectories from Table 1. The horizontal axis represents the starting times for NPVA and GS trajectories. The black dashed lines indicate the fractions of NPVA-GS and GS-NPVA trajectories within NPVA and GS trajectories respectively. The colored lines represent different airstreams within the NPVA-GS and GS-NPVA trajectories. The green lines indicate NPVA-WCB-GS and GS-WCB-NPVA, the orange lines indicate NPVA-DH-GS and GS-DH-NPVA, the blue lines indicate NPVA-CAO1-GS and GS-CAO1-NPVA, the teal lines indicate NPVA-CAO2-GS and GS-CAO2-NPVA, and the purple lines indicate NPVA-DI-GS and GS-DI-NPVA. LE0-3 refers to the starting dates of cyclones in Figure 2.

Characteristics of NPVA-GS and NPVA-nonGS trajectories. (a) Contributions of accumulated moisture uptakes to moisture present at the start of ascent (day 0) for NPVA-GS (orange line) and NPVA-nonGS (blue line) trajectories. Orange bars show the number of uptakes per day for NPVA-GS trajectories and dashed, blue bars for NPVA-nonGS trajectories. (b) Fraction of trajectories starting their ascent on a specific day, where day 0 represents the moment when they reach the upper-level NPVA.

Analysis of moisture sources for two different subsets of NPVA trajectories (Tab.1). (a) Mean composite of CAO index ( $\theta_{55T} - \theta_{850}$ ) for the period of 15 to 28 February (shading and contours), contours are plotted every 2 degrees from 2 to 20 K. (b) Mean composite of surface latent heat flux for the period of 15 to 28 February (shading), contours are plotted every 20  $W/m^2$ . Negative SLHF in the ERA5 dataset indicates that SLHF is from the ocean to the atmosphere. Sources of moisture for the NPVA-GS (left column) and NPVA-nonGS trajectories (right column). (c-d) The frequency of moisture uptakes per 3000  $km^2$ , (e-d) Moisture sources contribution to total moisture content prior to ascent ( $\%3000 km^2$ ).

The properties of the air parcels during moisture uptakes. (a) The fraction of all moisture uptakes for NPVA-GS trajectories at a given time, categorized by different regions: CAO – affected by the CAO event identified using the definition  $\theta_{55T} - \theta_{850} > 0$  K, CAO(2K) – affected by the CAO event identified using the definition  $\theta_{55T} - \theta_{850} > 2$  K, CS – cold sector of the cyclone, CAO&CS – identified as both CAO and the CS, rest – trajectories that are not CAO, CAO(2K), CS or CS&CAO, for all NPVA-GS trajectories at given time step between 6–27 Feb. 2019. (b) Average surface latent heat flux of the –orange NPVA-GS and blue –NPVA-nonGS trajectories at a given time from 6 to 27 February 2019, the 90th and 10th percentiles are plotted as light orange and blue shading, respectively. LE0-3 refers to starting dates of cyclones from Fig.??

Kernel Density Estimation (KDE; using Scott's rule; Scott (2015)) of air parcels distribution at the time when maximum value of surface latent heat flux is found along the trajectory (red contours), 24 h hours later (green contours) and when they start ascending (blue contours) (a) for trajectories started on 24 February at 21:00 UTC, (c) for all the NPVA-GS trajectories, (d) for all the NPVA-nonGS trajectories from 20–28 February 2019. Contours represent 10% steps of the density of air parcels. (b) The pressure change of trajectories started on 24 February at 21:00 UTC during ascent, together with moisture sources contribution to total moisture content prior to ascent as in Fig.?? (e-f).

Temporal evolution of: (a) pressure, (b) potential temperature, (c) surface latent heat flux, (d) surface sensible heat flux, (e) potential vorticity, (f) specific humidity along GS-NGPVA trajectories. Time 0 h refers to the start of the trajectory in the Gulf Stream region. The medians are represented as thick green lines and the 90th and 10th percentiles as light green shading.

Temporal evolution of: (a) potential vorticity, (b) pressure, (c) surface latent heat flux, (d) surface sensible heat flux, (e) potential temperature, (f) specific humidity along GS-NPVA-negPV trajectories (red) and GS-NPVA-posPV trajectories (blue). Trajectories are centered on the time step with maximum latent heating (hour 0). The medians are represented as thick red and blue lines and the 90th and 10th percentiles as light red and blue shading.

Vertical and horizontal distribution of negative potential vorticity over the area inside the green box in the plot (a) for 18 February 00:00 UTC. (a) Potential vorticity on the lowest model level and locations of air parcels with negative PV in the atmospheric boundary layer. (b) Vertical distribution of potential vorticity (shading) and liquid water content (green contours) averaged over the area between  $55^\circ - 60^\circ$  W and  $30^\circ - 45^\circ$  N, together with the location of all air parcels from the box that have

negative PV in the atmospheric boundary layer on 18 February 00:00 UTC. The plots were created using ERA5 data featuring a 1-hour time resolution.

1005 Schematic illustrating the ‘hand-over’ mechanism. Green line – Gulf Stream SST front, red lines – areas of intense sea-air heat and moisture exchange, purple lines – trajectories, blue lines – the advection of cold air. Consecutive cyclones are marked as LE1, LE2, L1, L2 (Fig.??). Gray contours represent surface pressure in intervals of 4 hPa and shading the surface latent heat flux on 20 February 12 UTC (a) and 21 February 18 UTC (b) (accumulated over a 3h period).

*Author contributions.* MW, CMG, LP, MF planned and designed the case study. MW analyzed the data and wrote the manuscript. CMG, LP,  
1010 MF gave important guidance during the project and provided feedback on the manuscript.

*Competing interests.* CMG and LP are members of the editorial board of Weather and Climate Dynamics. The authors have no other competing interests to declare.

*Acknowledgements.* We gratefully acknowledge the European Centre for Medium-Range Weather Forecasts (ECMWF) for providing the ERA5 reanalysis data set, which was made available through their website <http://www.ecmwf.int>. We also thank the members of the Large-  
1015 Scale Dynamics and Predictability group at KIT, as well as Jamie Mathews and Arnaud Czaja from Imperial College London, for their valuable discussions and contributions to this project. Additionally, we extend our thanks to Heini Wernli and Michael Sprenger for providing the Lagranto toolkit and cyclone dataset, which greatly facilitated our analyses. The contributions of MW and MF are funded by the German Research Foundation (DFG; Grant GR 5540/2-1) and the Swiss National Science Foundation (SNSF; Grant 200021E\_196978), respectively, as part of the Swiss-German collaborative project "The role of coherent air streams in shaping the Gulf stream’s impact on the large-scale  
1020 extratropical circulation (GULFimpact)." The contribution of CMG is funded by the Helmholtz Association as part of the Young Investigator Group "Sub-seasonal Predictability: Understanding the Role of Diabatic Outflow" (SPREADOUT, grant VH-NG-1243).



## References

- Aemisegger, F. and Papritz, L.: A Climatology of Strong Large-Scale Ocean Evaporation Events. Part I: Identification, Global Distribution, and Associated Climate Conditions, *J. Clim.*, 31, <https://doi.org/10.1175/JCLI-D-17-0591.1>, 2018.
- 1025 Athanasiadis, P., Ogawa, F., Omrani, N.-E., Keenlyside, N., Schiemann, R., Baker, A., Vidale, P., Bellucci, A., Ruggieri, P., Haarsma, R., Roberts, M., Roberts, C., Novak, L., and Gualdi, S.: Mitigating Climate Biases in the Midlatitude North Atlantic by Increasing Model Resolution: SST Gradients and Their Relation to Blocking and the Jet, *J. Clim.*, 35, 3385 – 3406, <https://doi.org/10.1175/JCLI-D-21-0515.1>, 2022.
- Attinger, R., Spreitzer, E., Boettcher, M., Richard, F., Wernli, H., and Joos, H.: Quantifying the role of individual diabatic processes for the formation of PV anomalies in a North Pacific cyclone, *Q. J. R. Meteorol. Soc.*, 145, 2454–2476, <https://doi.org/10.1002/qj.3573>, 2019.
- 1030 Attinger, R., Spreitzer, E., Boettcher, M., Wernli, H., and Joos, H.: Systematic assessment of the diabatic processes that modify low-level potential vorticity in extratropical cyclones, *Weather Clim. Dynam.*, 2, 1073–1091, <https://doi.org/10.5194/wcd-2-1073-2021>, 2021.
- Barriopedro, D., Fischer, E., Luterbacher, J., Trigo, R., and García-Herrera, R.: The Hot Summer of 2010: Redrawing the Temperature Record Map of Europe, *Science*, 332, 220–224, <https://doi.org/10.1126/science.1201224>, 2011.
- 1035 Binder, H., Böttcher, M., Joos, H., and Wernli, H.: The role of warm conveyor belts for the intensification of extratropical cyclones in Northern Hemisphere winter, *J. Atmos. Sci.*, 73, 3997–4020, <https://doi.org/10.1175/JAS-D-15-0302.1>, 2016.
- Binder, H., Boettcher, M., Joos, H., Sprenger, M., and Wernli, H.: Vertical cloud structure of warm conveyor belts – a comparison and evaluation of ERA5 reanalysis, CloudSat and CALIPSO data, *Weather Clim. Dynam.*, 1, 577–595, <https://doi.org/10.5194/wcd-1-577-2020>, 2020.
- 1040 Boutle, I., Belcher, S., and Plant, R.: Moisture transport in midlatitude cyclones, *Q. J. R. Meteorol. Soc.*, 137, 360–373, <https://doi.org/https://doi.org/10.1002/qj.783>, 2011.
- Browning, K.: The dry intrusion perspective of extra-tropical cyclone development, *Meteorol. Appl.*, 4, 317–324, <https://doi.org/10.1017/S1350482797000613>, 1997.
- Büeler, D., Ferranti, L., Magnusson, L., Quinting, J., and Grams, C.: Year-round sub-seasonal forecast skill for Atlantic–European weather regimes, *Q. J. R. Meteorol. Soc.*, 147, 4283–4309, <https://doi.org/10.1002/qj.4178>, 2021.
- 1045 Chagnon, J., Gray, S., and Methven, J.: Diabatic processes modifying potential vorticity in a North Atlantic cyclone, *Q. J. R. Meteorol. Soc.*, 139, 1270–1282, <https://doi.org/https://doi.org/10.1002/qj.2037>, 2013.
- Colucci, S.: Explosive Cyclogenesis and Large-Scale Circulation Changes: Implications for Atmospheric Blocking, *J. Atmos. Sci.*, 42, 2701 – 2717, [https://doi.org/10.1175/1520-0469\(1985\)042<2701:ECALSC>2.0.CO;2](https://doi.org/10.1175/1520-0469(1985)042<2701:ECALSC>2.0.CO;2), 1985.
- 1050 Colucci, S. and Alberta, T.: Planetary-Scale Climatology of Explosive Cyclogenesis and Blocking, *Mon. Weather Rev.*, 124, 2509 – 2520, [https://doi.org/10.1175/1520-0493\(1996\)124<2509:PSOEC>2.0.CO;2](https://doi.org/10.1175/1520-0493(1996)124<2509:PSOEC>2.0.CO;2), 1996.
- Crezee, B., Joos, H., and Wernli, H.: The Microphysical Building Blocks of Low-Level Potential Vorticity Anomalies in an Idealized Extratropical Cyclone, *J. Atmos. Sci.*, 74, 1403 – 1416, <https://doi.org/10.1175/JAS-D-16-0260.1>, 2017.
- Czaja, A., Frankignoul, C., Minobe, S., and Vannière, B.: Simulating the Midlatitude Atmospheric Circulation: What Might We Gain From High-Resolution Modeling of Air-Sea Interactions?, *Curr. Clim. Change Rep.*, 5, <https://doi.org/10.1007/s40641-019-00148-5>, 2019.
- 1055 Dacre, H., Clark, P., Martinez-Alvarado, O., Stringer, M., and Lavers, D.: How Do Atmospheric Rivers Form?, *Bull. Amer. Meteor.*, 96, 1243 – 1255, <https://doi.org/10.1175/BAMS-D-14-00031.1>, 2015.

- Dacre, H., Martínez-Alvarado, O., and Mbengue, C.: Linking Atmospheric Rivers and Warm Conveyor Belt Airflows, *J. Hydrometeorol.*, 20, 1183–1196, <https://doi.org/10.1175/JHM-D-18-0175.1>, 2019.
- 1060 Dae, J., Cannon, A., and Yu, B.: Influences of atmospheric blocking on North American summer heatwaves in a changing climate: a comparison of two Canadian Earth system model large ensembles, *Clim. Change*, 172, <https://doi.org/10.1007/s10584-022-03358-3>, 2022.
- de’Donato, F., Leone, M., Noce, D., Davoli, M., and Michelozzi, P.: The Impact of the February 2012 Cold Spell on Health in Italy Using Surveillance Data, *PLOS ONE*, 8, 1–9, <https://doi.org/10.1371/journal.pone.0061720>, 2013.
- Demirtaş, M.: The large-scale environment of the European 2012 high-impact cold wave: prolonged upstream and downstream atmospheric blocking, *Weather*, 72, 297–301, <https://doi.org/10.1002/wea.3020>, 2017.
- 1065 Eckhardt, S., Stohl, A., Wernli, H., James, P., Forster, C., and Spichtinger, N.: A 15-Year Climatology of Warm Conveyor Belts, *J. Clim.*, 17, 218 – 237, [https://doi.org/10.1175/1520-0442\(2004\)017<0218:AYCOWC>2.0.CO;2](https://doi.org/10.1175/1520-0442(2004)017<0218:AYCOWC>2.0.CO;2), 2004.
- Ferranti, L., Magnusson, L., Vitart, F., and Richardson, D.: How far in advance can we predict changes in large-scale flow leading to severe cold conditions over Europe?, *Q. J. R. Meteorol. Soc.*, 144, 1788–1802, <https://doi.org/10.1002/qj.3341>, 2018.
- 1070 Gao, Y., Leung, L., Lu, J., and Masato, G.: Persistent cold air outbreaks over North America in a warming climate, *Environ. Res. Lett.*, 10, <https://doi.org/10.1088/1748-9326/10/4/044001>, 2015.
- Grams, C. and Archambault, H.: The Key Role of Diabatic Outflow in Amplifying the Midlatitude Flow: A Representative Case Study of Weather Systems Surrounding Western North Pacific Extratropical Transition, *Mon. Weather. Rev.*, 144, 3847 – 3869, <https://doi.org/10.1175/MWR-D-15-0419.1>, 2016.
- 1075 Grams, C., Wernli, H., Böttcher, M., Čampa, J., Corsmeier, U., Jones, S., Keller, J., Lenz, C.-J., and Wiegand, L.: The key role of diabatic processes in modifying the upper-tropospheric wave guide: a North Atlantic case-study, *Q. J. R. Meteorol. Soc.*, 137, 2174–2193, <https://doi.org/10.1002/qj.891>, 2011.
- Grams, C., Beerli, R., Pfenninger, S., Staffell, I., and Wernli, H.: Balancing Europe’s wind-power output through spatial deployment informed by weather regimes, *Nat. Clim. Change*, 7, <https://doi.org/10.1038/nclimate3338>, 2017.
- 1080 Grams, C., Magnusson, L., and Madonna, E.: An Atmospheric Dynamics Perspective on the Amplification and Propagation of Forecast Error in Numerical Weather Prediction Models: A Case Study, *Q. J. R. Meteorol. Soc.*, 144, 2577–2591, <https://doi.org/10.1002/qj.3353>, 2018.
- Grumm, R.: The Central European and Russian Heat Event of July–August 2010, *Bull. Amer. Meteor. Soc.*, 92, 1285 – 1296, <https://doi.org/10.1175/2011BAMS3174.1>, 2011.
- Hauser, S., Teubler, F., Riemer, M., Knippertz, P., and Grams, C.: Towards a diagnostic framework unifying different perspectives on blocking dynamics: insight into a major blocking in the North Atlantic-European region, <https://doi.org/10.5194/wcd-2022-44>, preprint, 2022.
- 1085 Hawcroft, M., Shaffrey, L., Hodges, K., and Dacre, H.: How much Northern Hemisphere precipitation is associated with extratropical cyclones?, *Geophys. Res. Lett.*, 39, <https://doi.org/10.1029/2012GL053866>, 2012.
- Hersbach, H., Bell, B., et al.: The ERA5 global reanalysis, *Q. J. R. Meteorol. Soc.*, 146, 1999–2049, <https://doi.org/10.1002/qj.3803>, 2020.
- Hirata, H., Kawamura, R., Nonaka, M., and Tsuboki, K.: Significant Impact of Heat Supply From the Gulf Stream on a “Superbomb” Cyclone in January 2018, *Geophys. Res. Lett.*, 46, 7718–7725, <https://doi.org/10.1029/2019GL082995>, 2019.
- 1090 Ilotoviz, E., Ghate, V. P., and Raveh-Rubin, S.: The Impact of Slantwise Descending Dry Intrusions on the Marine Boundary Layer and Air-Sea Interface Over the ARM Eastern North Atlantic Site, *Journal of Geophysical Research: Atmospheres*, 126, <https://doi.org/10.1029/2020JD033879>, 2021.

- Jensen, J., Lee, S., Krummel, P., Katzfey, J., and Gogoasa, D.: Precipitation in marine cumulus and stratocumulus.: Part I: Thermodynamic and dynamic observations of closed cell circulations and cumulus bands, *Atmos. Res.*, 54, 117–155, [https://doi.org/10.1016/S0169-8095\(00\)00040-5](https://doi.org/10.1016/S0169-8095(00)00040-5), 2000.
- 1095 Joos, H. and R.M.Forbes: Impact of different IFS microphysics on a warm conveyor belt and the downstream flow evolution, *Q. J. R. Meteorol. Soc.*, 142, 2727–2739, <https://doi.org/10.1002/qj.2863>, 2016.
- Joos, H. and Wernli, H.: Influence of microphysical processes on the potential vorticity development in a warm conveyor belt: a case-study with the limited-area model COSMO, *Q. J. R. Meteorol. Soc.*, 138, 407–418, <https://doi.org/10.1002/qj.934>, 2012.
- 1100 Jullien, N., Vignon, E., Sprenger, M., Aemisegger, F., and Berne, A.: Synoptic conditions and atmospheric moisture pathways associated with virga and precipitation over coastal Adélie Land in Antarctica, *The Cryosphere*, 14, 1685–1702, <https://doi.org/10.5194/tc-14-1685-2020>, 2020.
- Kautz, L.-A., Martius, O., Pfahl, S., Pinto, J., Ramos, A., Sousa, P., and Woollings, T.: Atmospheric blocking and weather extremes over the Euro-Atlantic sector – a review, *Weather Clim. Dynam.*, 3, 305–336, <https://doi.org/10.5194/wcd-3-305-2022>, 2022.
- 1105 Kwon, Y., Alexander, M., Bond, N., Frankignoul, C., Nakamura, H., Qiu, B., and Thompson, L.: Role of the Gulf Stream and Kuroshio–Oyashio Systems in Large-Scale Atmosphere–Ocean Interaction: A Review, *J. Clim.*, 23, 3249 – 3281, <https://doi.org/10.1175/2010JCLI3343.1>, 2010.
- Kwon, Y.-O., Seo, H., Ummenhofer, C., and Joyce, T.: Impact of Multidecadal Variability in Atlantic SST on Winter Atmospheric Blocking, *J. Clim.*, 33, 867 – 892, <https://doi.org/10.1175/JCLI-D-19-0324.1>, 2020.
- 1110 Leach, N., Weisheimer, A., Allen, M., and Palmer, T.: Forecast-based attribution of a winter heatwave within the limit of predictability, *PNAS*, 118, e2112087 118, <https://doi.org/10.1073/pnas.2112087118>, 2021.
- Lupo, A. and Smith, J.: Climatological features of blocking anticyclones in the Northern Hemisphere, *Tellus A: Dyn. Meteorol. Oceanogr.*, 47, 439–456, <https://doi.org/10.3402/tellusa.v47i4.11527>, 1995.
- 1115 Madonna, E., Wernli, H., Joos, H., and Martius, O.: Warm Conveyor Belts in the ERA-Interim Dataset (1979–2010). Part I: Climatology and Potential Vorticity Evolution, *J. Clim.*, 27, 3–26, <https://doi.org/10.1175/JCLI-D-12-00720.1>, 2014.
- Matsueda, M. and Palmer, T.: Estimates of flow-dependent predictability of wintertime Euro-Atlantic weather regimes in medium-range forecasts, *Q. J. R. Meteorol. Soc.*, 144, 1012–1027, <https://doi.org/10.1002/qj.3265>, 2018.
- Methven, J.: Potential vorticity in warm conveyor belt outflow, *Q. J. R. Meteorol. Soc.*, 141, 1065–1071, <https://doi.org/10.1002/qj.2393>, 2015.
- 1120 Michel, S., Heydt, A., Westen, R., Baatsen, M., and Dijkstra, H.: Increased wintertime European atmospheric blocking frequencies in General Circulation Models with a coupled eddy-permitting ocean, *npj Clim. Atmos. Sci.*, 6, <https://doi.org/10.21203/rs.3.rs-1811560/v1>, 2023.
- Moore, G. and Renfrew, I.: An Assessment of the Surface Turbulent Heat Fluxes from the NCEP–NCAR Reanalysis over the Western Boundary Currents, *J. Clim.*, 15, 2020 – 2037, [https://doi.org/10.1175/1520-0442\(2002\)015<2020:AAOTST>2.0.CO;2](https://doi.org/10.1175/1520-0442(2002)015<2020:AAOTST>2.0.CO;2), 2002.
- 1125 Mullen, S.: Transient Eddy Forcing of Blocking Flows, *J. Atmos. Sci.*, 44, 3 – 22, [https://doi.org/10.1175/1520-0469\(1987\)044<0003:TEFOBF>2.0.CO;2](https://doi.org/10.1175/1520-0469(1987)044<0003:TEFOBF>2.0.CO;2), 1987.
- Nakamura, H. and Wallace, J.: Synoptic Behavior of Baroclinic Eddies during the Blocking Onset, *Mon. Weather Rev.*, 121, 1892 – 1903, [https://doi.org/10.1175/1520-0493\(1993\)121<1892:SBOBED>2.0.CO;2](https://doi.org/10.1175/1520-0493(1993)121<1892:SBOBED>2.0.CO;2), 1993.
- Nakamura, H., Sampe, T., Goto, A., Ohfuchi, W., and Xie, S.: On the importance of midlatitude oceanic frontal zones for the mean state and dominant variability in the tropospheric circulation, *Geophys. Res. Lett.*, 35, <https://doi.org/10.1029/2008GL034010>, 2008.
- 1130

- Novak, L., Ambaum, M., and Tailleux, R.: The Life Cycle of the North Atlantic Storm Track, *J. Atmos. Sci.*, 72, 821 – 833, <https://doi.org/10.1175/JAS-D-14-0082.1>, 2015.
- Omrani, N.-E., Ogawa, F., Nakamura, H., Keenlyside, N., Lubis, S., and Matthes, K.: Key Role of the Ocean Western Boundary currents in shaping the Northern Hemisphere climate, *Scientific Reports*, 9, <https://doi.org/10.1038/s41598-019-39392-y>, 2019.
- 1135 O'Reilly, C., Minobe, S., Kuwano-Yoshida, A., and Woollings, T.: The Gulf Stream influence on wintertime North Atlantic jet variability, *Q. J. R. Meteorol. Soc.*, 143, 173–183, <https://doi.org/10.1002/qj.2907>, 2017.
- Painemal, D., Corral, A., Sorooshian, A., M.A.Brunke, et al.: An Overview of Atmospheric Features Over the Western North Atlantic Ocean and North American East Coast—Part 2: Circulation, Boundary Layer, and Clouds, *J. Geophys. Res. Atmos.*, 126, e2020JD033423, <https://doi.org/10.1029/2020JD033423>, 2021.
- 1140 Paluch, I. R. and Lenschow, D. H.: Stratiform Cloud Formation in the Marine Boundary Layer, *J. Atmos. Sci.*, 48, 2141–2158, [https://doi.org/10.1175/1520-0469\(1991\)0482.0.CO;2](https://doi.org/10.1175/1520-0469(1991)0482.0.CO;2), 1991.
- Pang, B., Lu, R., and Ren, R.: Influence of Siberian Blocking on Long-Lived Cold Surges over the South China Sea, *J. Clim.*, 33, 6945–6956, <https://doi.org/10.1175/JCLI-D-19-0944.1>, 2020.
- Papritz, L. and Grams, C.: Linking Low-Frequency Large-Scale Circulation Patterns to Cold Air Outbreak Formation in the Northeastern North Atlantic, *Geophys. Res. Lett.*, 45, 2542–2553, <https://doi.org/10.1002/2017GL076921>, 2018.
- 1145 Papritz, L. and Spengler, T.: Analysis of the slope of isentropic surfaces and its tendencies over the North Atlantic, *Q. J. R. Meteorol. Soc.*, 141, 3226–3238, <https://doi.org/10.1002/qj.2605>, 2015.
- Papritz, L. and Spengler, T.: A Lagrangian Climatology of Wintertime Cold Air Outbreaks in the Irminger and Nordic Seas and Their Role in Shaping Air–Sea Heat Fluxes, *J. Clim.*, 30, 2717 – 2737, <https://doi.org/10.1175/JCLI-D-16-0605.1>, 2017.
- 1150 Papritz, L., Pfahl, S., Sodemann, H., and Wernli, H.: A Climatology of Cold Air Outbreaks and Their Impact on Air–Sea Heat Fluxes in the High-Latitude South Pacific, *J. Clim.*, 28, 342 – 364, <https://doi.org/10.1175/JCLI-D-14-00482.1>, 2015.
- Papritz, L., Aemisegger, F., and Wernli, H.: Sources and Transport Pathways of Precipitating Waters in Cold-Season Deep North Atlantic Cyclones, *J. Atmos. Sci.*, 78, 3349–3368, <https://doi.org/10.1175/JAS-D-21-0105.1>, 2021.
- Pfahl, S., Madonna, E., Boettcher, M., Joos, H., and Wernli, H.: Warm Conveyor Belts in the ERA-Interim Dataset (1979–2010). Part II: Moisture Origin and Relevance for Precipitation, *J. Clim.*, 27, 27–40, <https://doi.org/10.1175/JCLI-D-13-00223.1>, 2014.
- 1155 Pfahl, S., Schwiertz, C., Croci-Maspoli, M., Grams, C., and Wernli, H.: Importance of latent heat release in ascending air streams for atmospheric blocking, *Nat. Geosci.*, 8, 610–614, <https://doi.org/10.1038/ngeo2487>, 2015.
- Raveh-Rubin, S.: Dry Intrusions: Lagrangian Climatology and Dynamical Impact on the Planetary Boundary Layer, *J. Clim.*, 30, 6661–6682, <https://doi.org/10.1175/JCLI-D-16-0782.1>, 2017.
- 1160 Reed, R., Stoelinga, M., and Kuo, Y.-H.: A model-aided study of the origin and evolution of the anomalously high potential vorticity in the inner region of a rapidly deepening marine cyclone, *Mon. Weather Rev.*, 120, 893–913, [https://doi.org/10.1175/1520-0493\(1992\)120<0893:AMASOT>2.0.CO;2](https://doi.org/10.1175/1520-0493(1992)120<0893:AMASOT>2.0.CO;2), 1992.
- Sanders, F. and Gyakum, J.: Synoptic-dynamic climatology of the ‘bomb’, [https://doi.org/10.1175/1520-0493\(1980\)108<1589:SDCOT>2.0.CO;2](https://doi.org/10.1175/1520-0493(1980)108<1589:SDCOT>2.0.CO;2), 1980.
- 1165 Scaife, A., Copesey, D., Gordon, C., Harris, C., Hinton, T., Keeley, S., O'Neill, A., Roberts, M., and Williams, K.: Improved Atlantic winter blocking in a climate model, *Geophys. Res. Lett.*, 38, <https://doi.org/10.1029/2011GL049573>, 2011.
- Scott, D.: Multivariate density estimation: Theory, practice, and visualization: Second edition, <https://doi.org/10.1002/9781118575574>, 2015.

- Shaw, T., Baldwin, M., Barnes, E., Caballero, R., Garfinkel, C., Hwang, Y.-T., Li, C., O’Gorman, P., et al.: Storm track processes and the opposing influences of climate change, *Nat. Geosci.*, 9, <https://doi.org/10.1038/ngeo2783>, 2016.
- 1170 Sheldon, L., Czaja, A., Vanni re, B., Morcrette, C., Sohet, B., Casado, M., and Smith, D.: A ‘warm path’ for Gulf Stream–troposphere interactions, *Tellus A: Dyn. Meteorol. Oceanogr.*, 69, 1299–1397, <https://doi.org/10.1080/16000870.2017.1299397>, 2017.
- Sodemann, H. and Stohl, A.: Moisture Origin and Meridional Transport in Atmospheric Rivers and Their Association with Multiple Cyclones, *Mon. Weather. Rev.*, 141, 2850 – 2868, <https://doi.org/10.1175/MWR-D-12-00256.1>, 2013.
- Sodemann, H., Schwierz, C., and Wernli, H.: Interannual variability of Greenland winter precipitation sources: Lagrangian moisture diagnostic and North Atlantic Oscillation influence, *J. Geophys. Res.*, 113, <https://doi.org/10.1029/2007JD008503>, 2008.
- 1175 Spensberger, C., Madonna, E., Boettcher, M., Grams, C., Papritz, L., Quinting, J., R thlisberger, M., Sprenger, M., and Zschenderlein, P.: Dynamics of Concurrent and Sequential Central European and Scandinavian Heatwaves, *Q. J. R. Meteorol. Soc.*, 146, 2998–3013, <https://doi.org/10.1002/qj.3822>, 2020.
- Sprenger, M.: Global climatologies of Eulerian and Lagrangian flow features based on ERA-Interim, *Bull. Amer. Meteor. Soc.*, 98, 1739–1748, 2017.
- 1180 Sprenger, M. and Wernli, H.: The LAGRANTO Lagrangian analysis tool – version 2.0, *Geosci. Model Dev.*, 8, 2569–2586, <https://doi.org/10.5194/gmd-8-2569-2015>, 2015.
- Steinfeld, D. and Pfahl, S.: The role of latent heating in atmospheric blocking dynamics: a global climatology, *Clim. Dyn.*, 53, <https://doi.org/10.1007/s00382-019-04919-6>, 2019.
- 1185 Steinfeld, D., Boettcher, M., Forbes, R., and Pfahl, S.: The sensitivity of atmospheric blocking to upstream latent heating – numerical experiments, *Weather Clim. Dynam.*, 1, 405–426, <https://doi.org/10.5194/wcd-1-405-2020>, 2020.
- Teubler, F. and Riemer, M.: Dynamics of Rossby Wave Packets in a Quantitative Potential Vorticity–Potential Temperature Framework, *J. Atmos. Sci.*, 73, 1063 – 1081, <https://doi.org/10.1175/JAS-D-15-0162.1>, 2016.
- Tilinina, N., Gavrikov, A., and Gulev, S.: Association of the North Atlantic Surface Turbulent Heat Fluxes with Midlatitude Cyclones, *Mon. Weather. Rev.*, 146, 3691 – 3715, <https://doi.org/10.1175/MWR-D-17-0291.1>, 2018.
- 1190 Vanni re, B., Czaja, A., and Dacre, H.: Contribution of the cold sector of extratropical cyclones to mean state features over the Gulf Stream in winter, *Q. J. R. Meteorol. Soc.*, 143, 1990–2000, <https://doi.org/10.1002/qj.3058>, 2017a.
- Vanni re, B., Czaja, A., Dacre, H., and Woollings, T.: A ‘Cold Path’ for the Gulf Stream–Troposphere Connection, *J. Clim.*, 30, 1363–1379, <https://doi.org/10.1175/JCLI-D-15-0749.1>, 2017b.
- 1195  ampa, J. and Wernli, H.: A PV perspective on the vertical structure of mature midlatitude cyclones in the northern hemisphere, *J. Atmos. Sci.*, 69, 725–740, <https://doi.org/10.1175/JAS-D-11-050.1>, 2012.
- Wazneh, H., Gachon, P., deVernal, A., Laprise, R., and Tremblay, B.: Atmospheric blocking events in the North Atlantic: trends and links to climate anomalies and teleconnections, *Clim. Dyn.*, 56, <https://doi.org/10.1007/s00382-020-05583-x>, 2021.
- Wernli, H. and Davies, H.: A Lagrangian-based analysis of extratropical cyclones, I, The method and some applications., *Q. J. R. Meteorol. Soc.*, 123, 467–489, <https://doi.org/10.1002/qj.49712353811>, 1997.
- 1200 Wernli, H. and Schwierz, C.: Surface cyclones in the ERA-40 dataset (1958–2001). Part I: Novel identification method and global climatology, *J. Atmos. Sci.*, 63, 2486–2507, 2006.
- Wood, R.: Drizzle in Stratiform Boundary Layer Clouds. Part I: Vertical and Horizontal Structure, *J. Atmos. Sci.*, 62, 3011–3033, <https://doi.org/10.1175/JAS3529.1>, 2005.

- 1205 Xin, F., Peng, D., Liu, R., and Liu, S.-C.: Moisture sources for the weather pattern classified extreme precipitation in the first rainy season over South China, *Int. J. Climatol.*, 42, 6027–6041, <https://doi.org/10.1002/joc.7576>, 2022.
- Yamamoto, A., Nonaka, M., Martineau, P., Yamazaki, A., Kwon, Y.-O., Nakamura, H., and Taguchi, B.: Oceanic moisture sources contributing to wintertime Euro-Atlantic blocking, *WCD*, 2, 819–840, <https://doi.org/10.5194/wcd-2-819-2021>, 2021.
- Yamazaki, A. and Itoh, H.: Selective absorption mechanism for the maintenance of blocking, *Geophys. Res. Lett.*, 36, <https://doi.org/10.1029/2008GL036770>, 2009.
- 1210 Young, M. and Galvin, J.: The record-breaking warm spell of February 2019 in Britain, the Channel Islands, France and the Netherlands, *Weather*, 75, 36–45, <https://doi.org/10.1002/wea.3664>, 2020.
- Zhuo, W., Yao, Y., Luo, D., Simmonds, I., and Huang, F.: Combined impact of the cold vortex and atmospheric blocking on cold outbreaks over East Asia and the potential for short-range prediction of such occurrences, *Environ. Res. Lett.*, 17, 084037, <https://doi.org/10.1088/1748-9326/ac8362>, 2022.
- 1215

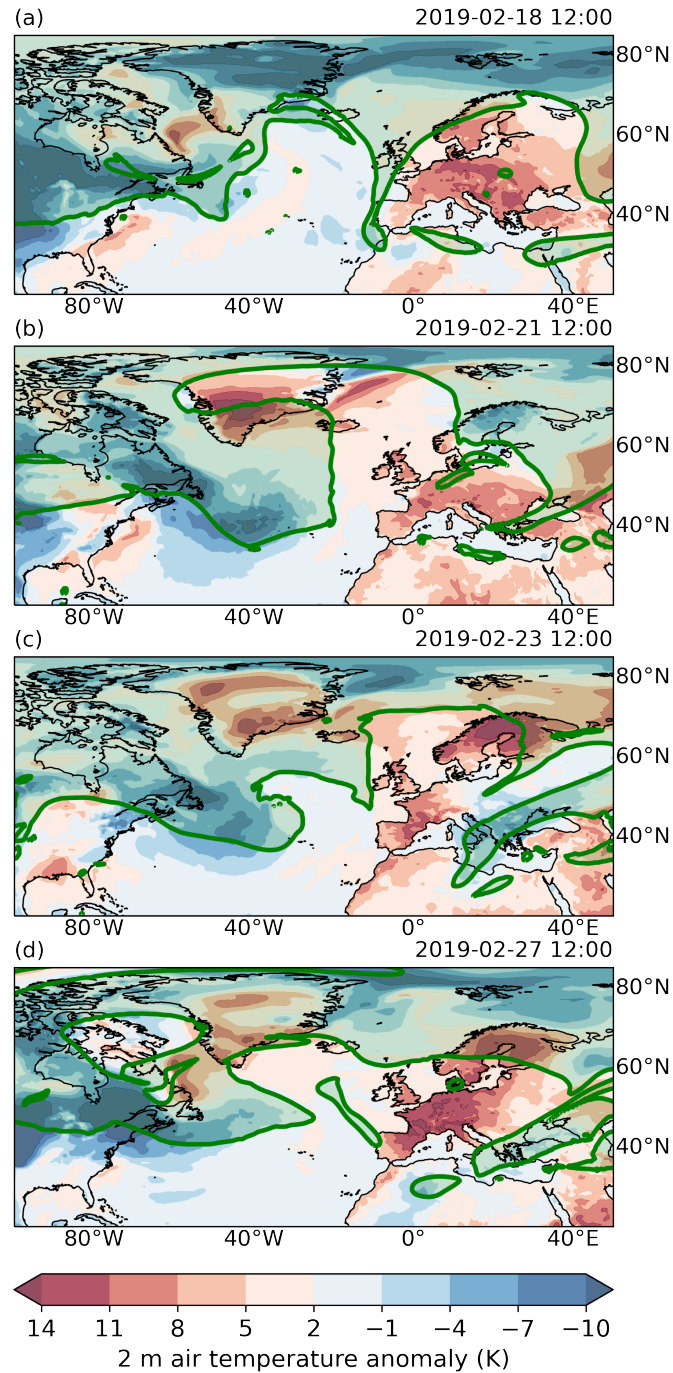


**Figure 1.** 2 m temperature anomalies (with respect to a 30d running mean, shading) and upper-level 2 PVU contour at 315 K (green line), with PV values higher than 2 PVU shaded in green. Panels are for 12:00 UTC on 18 February 2019 (a), 21 February 2019 (b), 23 February 2019 (c), and 27 February 2019 (d).

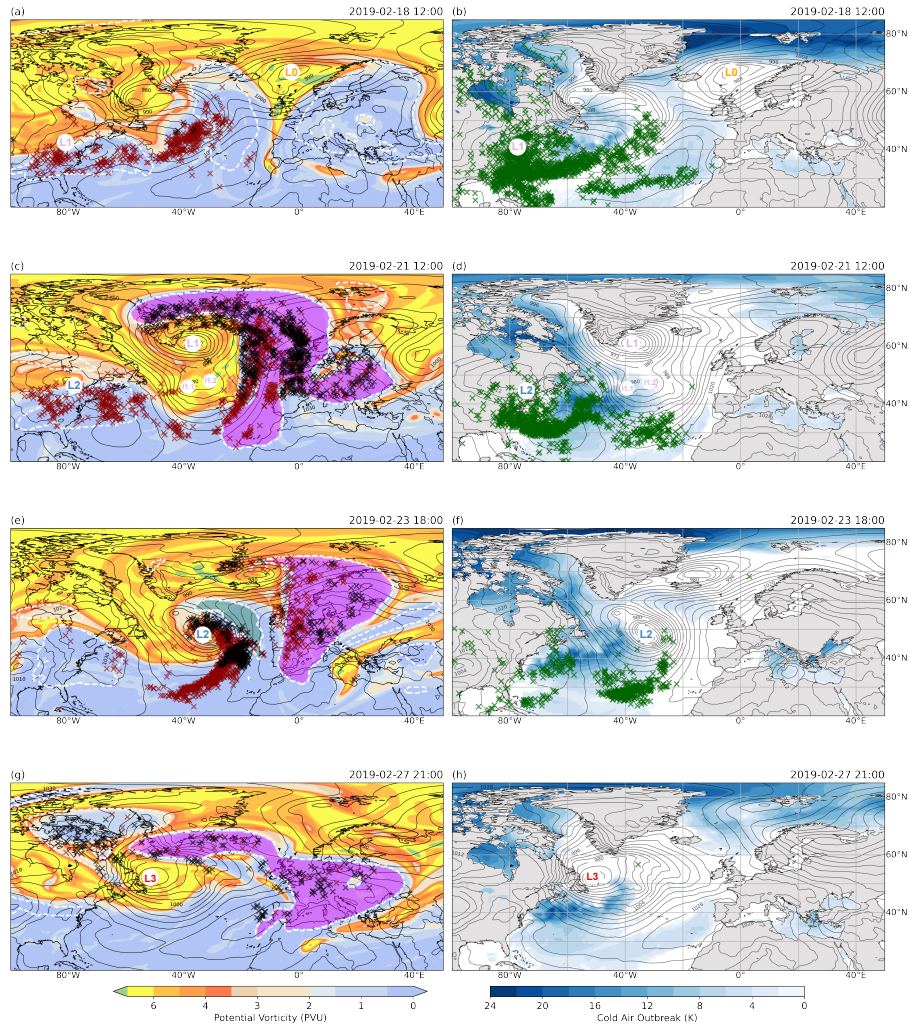


**Figure 2.** Synoptic evolution of European Blocking episode from February 2019. First column: potential vorticity (shading, PVU) at 315 K and negative potential vorticity anomaly (NPVA) objects (white dashed contours). The major NPVA is shaded in magenta and the minor in light green (Section 2.1.3). Black crosses represent the location of every 30th NPVA GS air parcel at the outflow stage ( $p > 400$  hPa) at the valid time of the panel. Red crosses indicate the locations of every 30th NPVA GS air parcel during the ascent stage ( $400 \text{ hPa} < p < 800 \text{ hPa}$ ) for the same timestamp. Second column: Cold air outbreak index (shading, K). Green crosses denote the positions of every 30th NPVA GS air parcel at the inflow stage ( $p > 800$  hPa) for the corresponding time. Panels are shown for 12:00 UTC 18 February 2019 (a, b), 12:00 UTC 21 February 2019 (c, d), 18:00 UTC 23 February 2019 (e, f), and 21:00 UTC 27 February 2019 (g, h). Black contours in both columns show mean sea level pressure (hPa) and labels L0-L4 refer to the mentioned cyclones with their tracks shown in Fig.3.



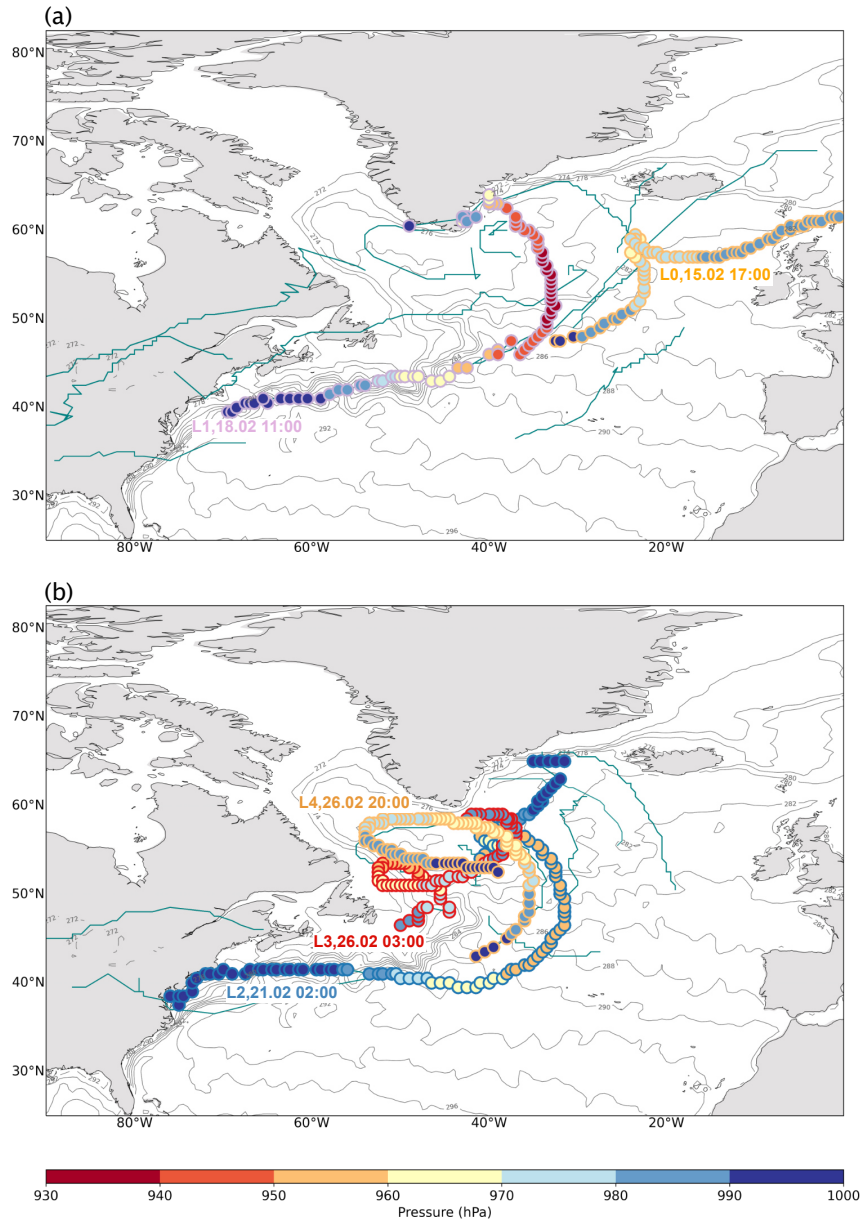


**Figure 3.** Tracks of cyclones with genesis in the North Atlantic between 15-20 February 2019 (a) and 20-28 February 2019 (b) with contours representing the average sea surface temperature during that period, which serves as an indicator of the Gulf Stream's gradient position. The tracks of rapidly intensifying cyclones (L0-L4, (Sanders and Gyakum, 1980)) are shown by colored circles with the interior color representing minimum sea level pressure. The date near a cyclone's identifier (L0-L4) refers to the genesis time. The tracks of other, non-rapidly intensifying cyclones are shown by thin blue lines.

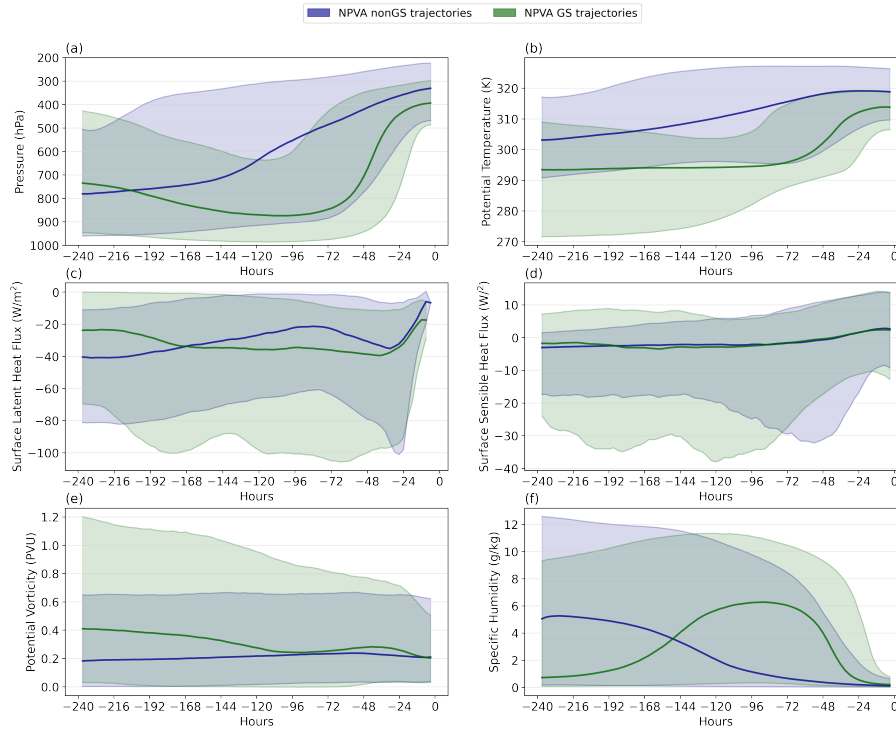


**Figure 4.** Temporal evolution of (a) pressure, (b) potential temperature, (c) surface latent heat flux, (d) surface sensible heat flux, (e) potential vorticity, (f) specific humidity along NPVA GS (green) and NPVA nonGS (blue) trajectories. Time 0 h refers to the start of the backward trajectory in the NPVA object. The medians are represented as thick lines and the 10th to 90th percentile range is shaded in light green/light blue.

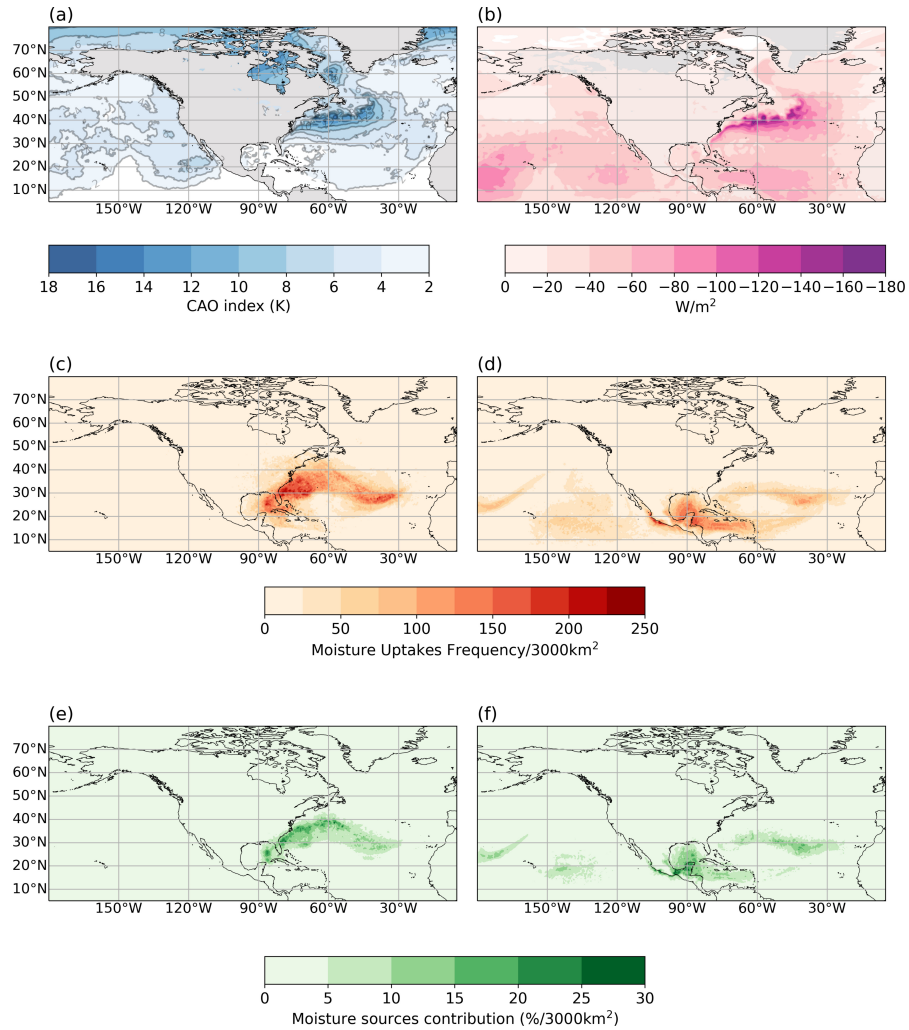


**Figure 5.** (a) Mean of the 3-hourly CAO index ( $\theta_{SSST} - \theta_{850}$ ) during the period from 15 to 28 February 2019 (shading and contours), contours are plotted every 2 K from 2 to 20 K. (b) Same as (a) but for surface latent heat flux (SLHF, shading). Negative SLHF in the ERA5 dataset indicates that SLHF is from the ocean to the atmosphere. (c-f) Analysis of moisture sources for NPVA GS (left column) and NPVA nonGS trajectories (right column; Tab.1). Panels (c, d) show the frequency of moisture uptakes per 3000 km<sup>2</sup> and panels (e, f) the moisture sources contribution to total moisture content present in the trajectory prior to ascent (%/3000 km<sup>2</sup>).

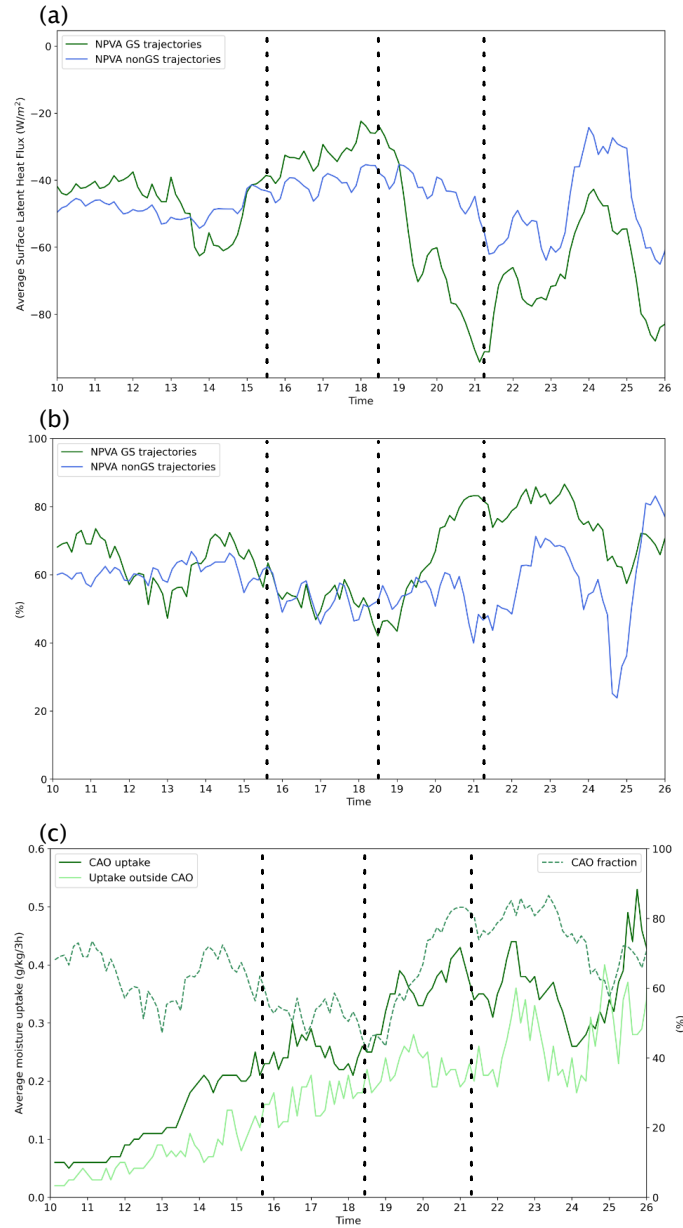


**Figure 6.** Properties of the air parcels during moisture uptakes. (a) Average surface latent heat flux at the locations of moisture uptakes occurring at the times indicated on the x-axis. The green line represents NPVA GS trajectories, while the blue line denotes NPVA nonGS trajectories. (b) Fraction of moisture uptakes taking place in the CAO regions ( $\theta_{SST} - \theta_{850}$ ), colors correspond to those in (a). (c) Average moisture uptake ( $\Delta q = q_t - q_{t+3h}$ ) for the time specified on the x-axis. The dark green line represents uptakes for NPVA GS trajectories within CAO, while the light green line represents uptakes outside of CAO regions. The green dashed line indicates the fraction of moisture uptakes occurring within CAO regions for NPVA GS trajectories as in (b). Vertical dashed lines refer to cyclogenesis times of cyclones (from left to right): L0, L1, L2 (Fig.3)

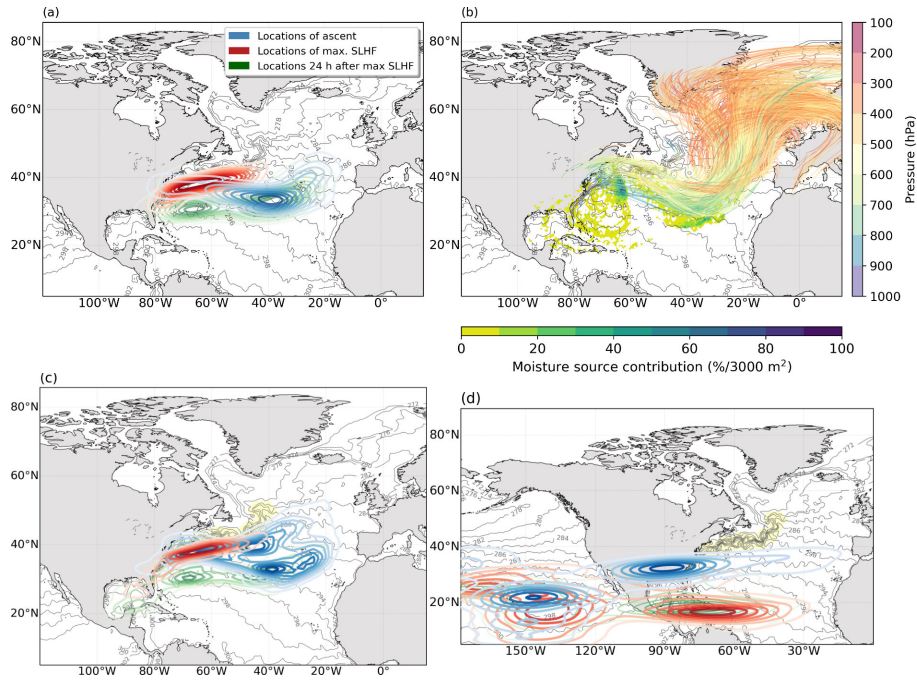


**Figure 7.** Kernel Density Estimation (KDE; using Scott's rule; Scott (2015)) of air parcel locations at the time of maximum upward surface latent heat flux along trajectories (red contours), 24 h hours later (green contours) and when they start ascending (blue contours) (a) for NPVA GS trajectories started on 24 February at 21:00 UTC, and (c,d) for all trajectories started between 20-28 February 2019 for (c) all the NPVA GS trajectories and for (d) all the NPVA nonGS trajectories. Contours represent 10% steps of the density of air parcels. (b) NPVA GS trajectories started on 24 February at 21:00 UTC colored in pressure height, together with moisture sources' contribution to total moisture present at the time of the start of ascent.

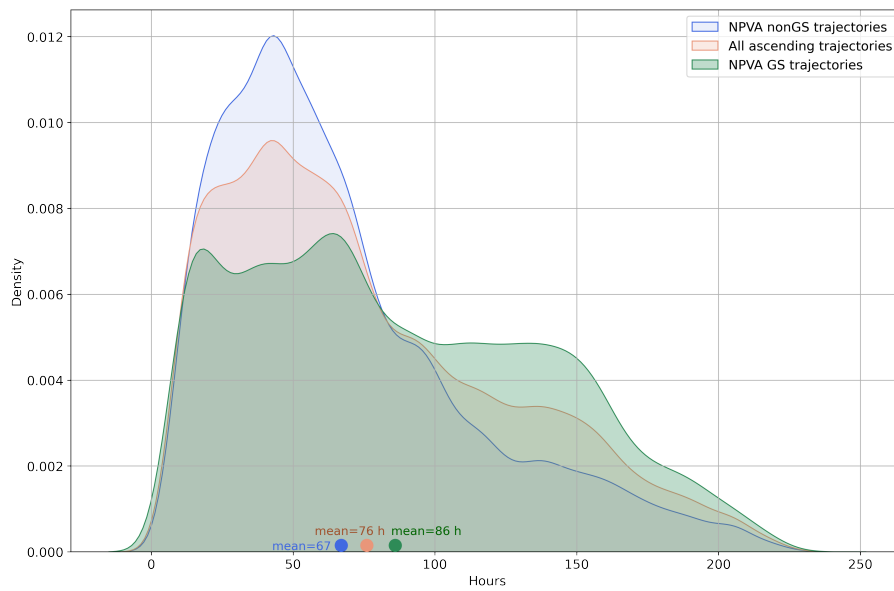


**Figure 8.** Probability distribution function of the time difference between the strongest moisture uptake and the point at which the pressure decreases to below 800 hPa during the ascent (start of ascent), for NPVA (orange), NPVA GS (green) and NPVA nonGS (blue) trajectories (Tab.1). Dots with labels represent mean values for each set of trajectories.

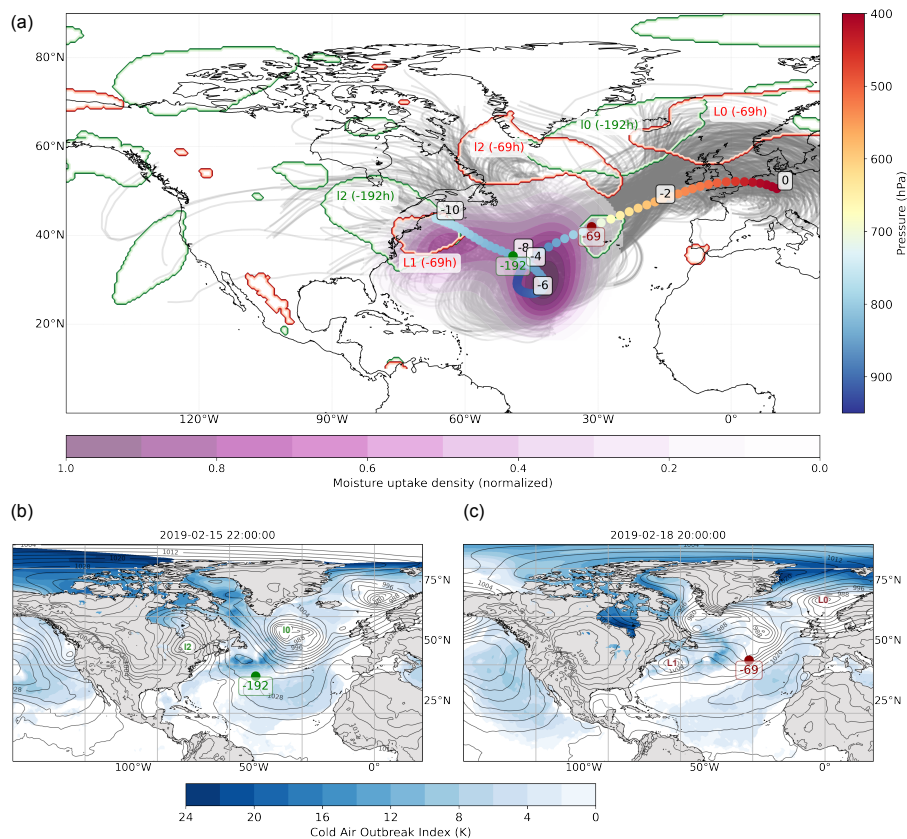


**Figure 9.** 10-day backward trajectories initialized on 21 February 2019 at 12:00 UTC. (a) Colored dots represent the mean location and pressure (hPa) of trajectories crossing the latitude of 30°N and longitude of 50°W (to southeast), while light grey lines represent individual trajectories used for the calculation of the mean. Black labels mark days prior to arrival in the upper-level NPVA. The green dot (with its corresponding green label) indicates the average moisture uptake time (in hours) for the displayed trajectories, and the green contours outline cyclones present at that moment. The red dot (with its corresponding red label) indicates the average time of start of ascent (in hours) for the displayed trajectories, and the red contours outline cyclones present at that moment. Purple shading represents the normalized (0-1) density of the trajectory positions at the time of most intense moisture uptake. (b) Cold Air Outbreak Index (K) (shading) and mean sea level pressure at the average time of most intense uptake (-192 h), (c) same as (b) but for the average time of start of ascent (-69 h).

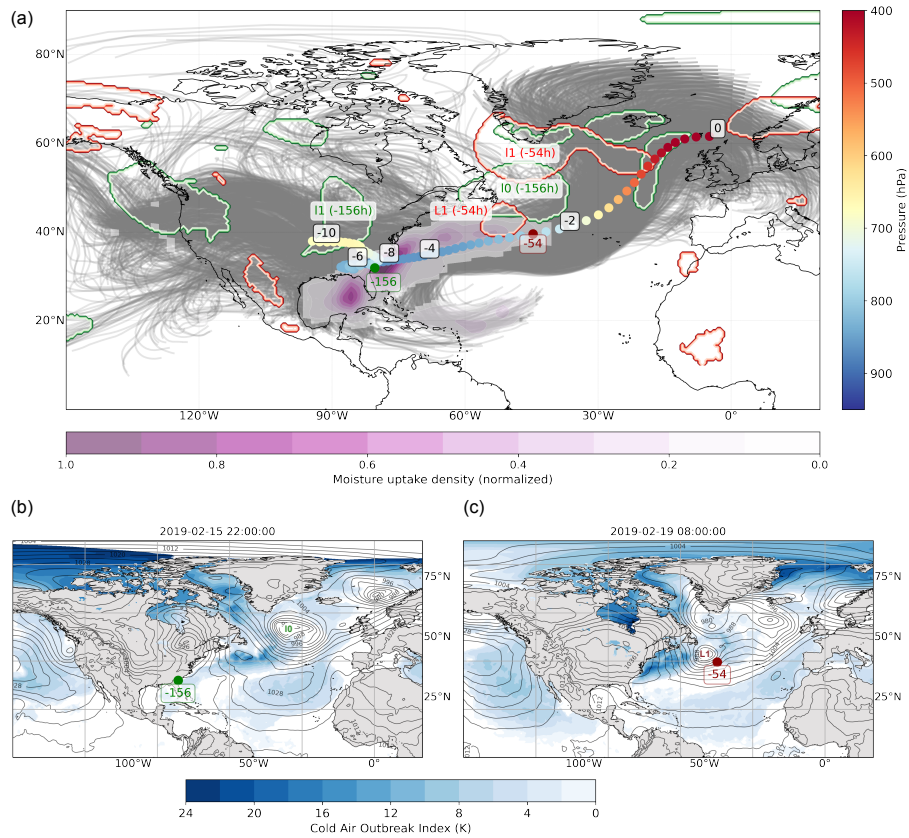


**Figure 10.** Same as Fig.9 but for trajectories that do not cross over latitude of 30°N and longitude of 50°W.



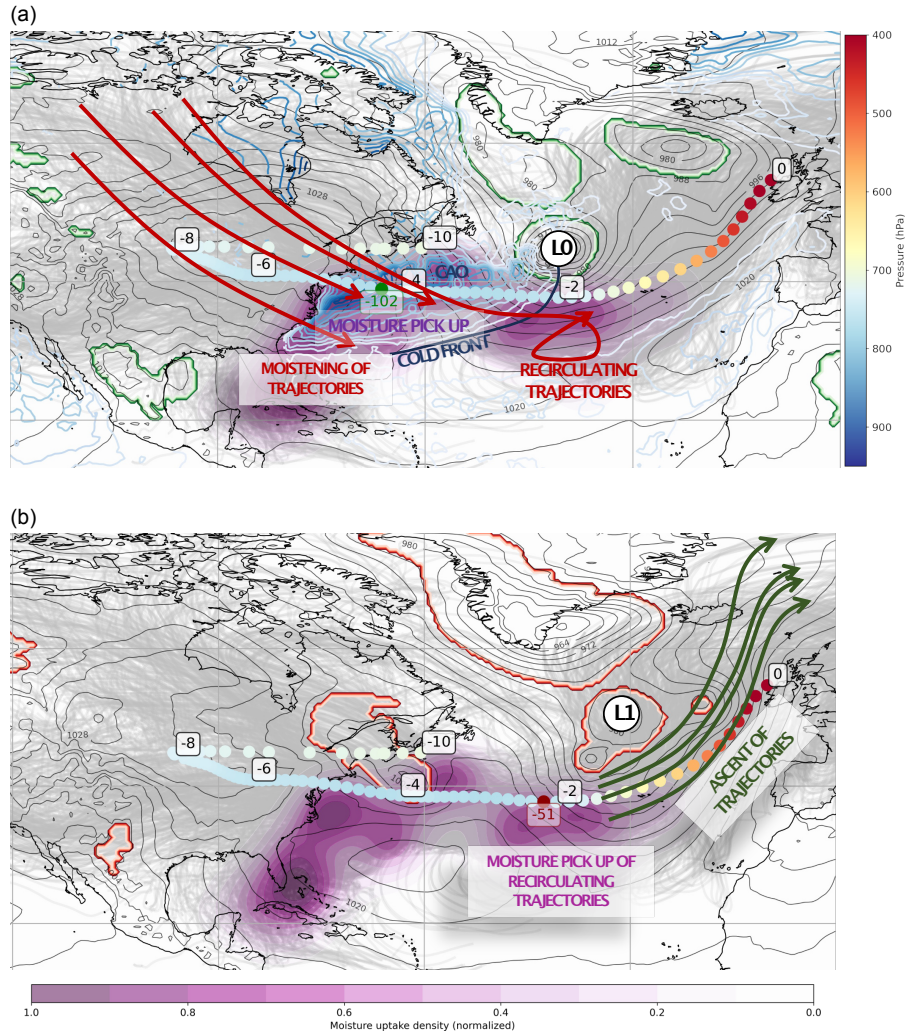


**Figure 11.** Schematic illustrating the link between cyclones and the pathways of NPVA GS trajectories based on the trajectories initiated from the upper-level NPVA on 24 February at 00:00 UTC. (a) The synoptic situation at the average moisture pick-up time, on 19 February at 18:00 UTC. Black contours depict the mean sea level pressure (hPa), green contours represent cyclone masks, purple shading indicates the normalized density of moisture uptake locations, and blue contours show the cold air outbreak index (K). (b) same as (a) but corresponding to the average start time of trajectory ascent on 21 February at 21:00 UTC, with red contours highlighting cyclone masks.

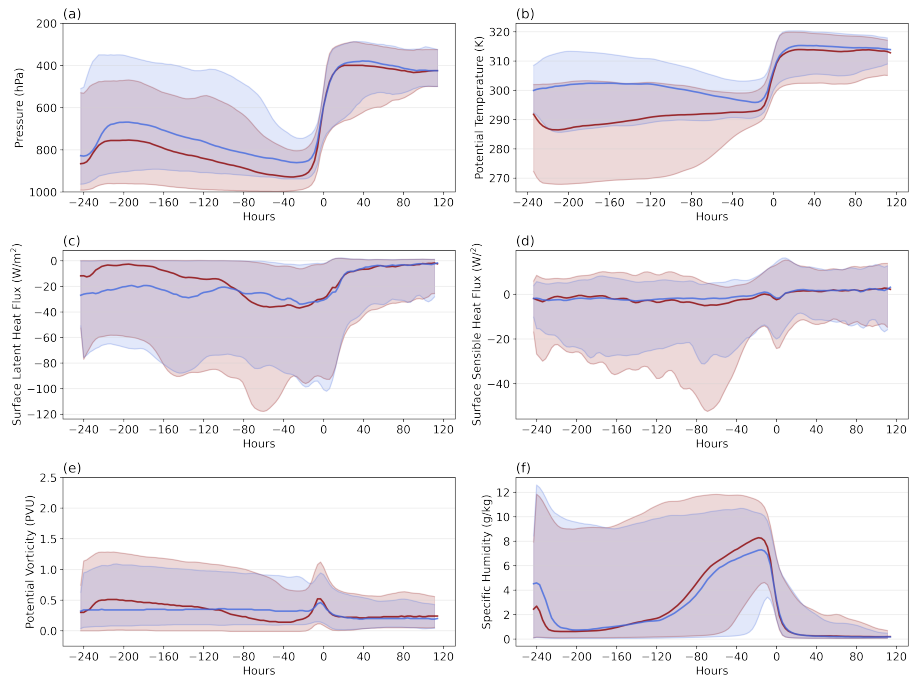


**Figure A1.** Temporal evolution of: (a) potential vorticity, (b) pressure, (c) surface latent heat flux, (d) surface sensible heat flux, (e) potential temperature, (f) specific humidity along NPVA GS trajectories with negative PV in the atmospheric boundary layer (at least one time step) (red) and with only positive PV (blue). Trajectories are centered on the time step with maximum latent heating (hour 0). The medians are represented as thick red and blue lines and the 90th and 10th percentiles as light red and blue shading.

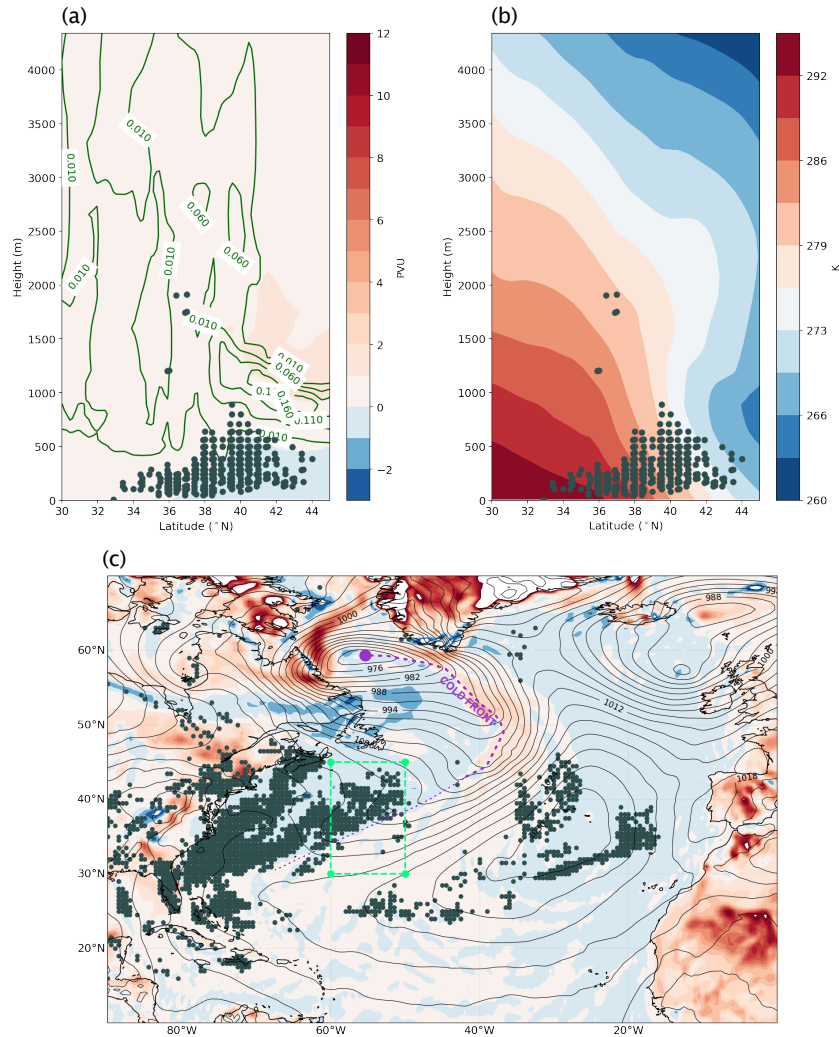


**Figure A2.** Vertical and horizontal distribution of negative potential vorticity and potential temperature over the area inside the green box in the plot (a) on 18 February at 00:00 UTC. (a) Vertical distribution of potential vorticity (shading) and liquid water content (green contours) averaged over the area between 55° - 60° W and 30° - 45° N, together with the location of all air parcels from the box that have negative PV in the atmospheric boundary layer on 18 February 00:00 UTC. (b) Same as (a) but the contours represent the vertical distribution of potential temperature (shading) averaged over the area between 55° - 60° W and 30° - 45° N. (c) Potential vorticity on the lowest model level and locations of air parcels with negative PV in the atmospheric boundary layer. The plots were created using ERA5 data featuring a 1-hour time resolution.